Bachelorarbeit Physik 24. Juli 2016

Realization of the "Precision Optical Calibration Module" prototype for calibration of IceCube-Gen2

Andreas Gärtner

Erstkorrektor Prof. Elisa Resconi
Zweitkorrektor Prof. Bastian Märkisch

Technische Universität München
Fakultät für Physik

Abstract

The IceCube Neutrino Observatory is a cubic kilometer neutrino detector in the Antarctic ice at the South Pole. The planned extension IceCube-Gen2 contains the Precision IceCube Next Generation Upgrade (PINGU) that will limit the energy threshold of IceCube and is designed for the detection of atmospheric neutrino oscillations. For PINGU a calibration device is needed that can be deployed in the Antarctic ice and will allow the low energy calibration (GeV range) for precise measurements of atmospheric neutrinos.

The Precision Optical Calibration Module (POCAM) is an isotropic light source emitting a short light pulse that can be used to calibrate the photomultiplier tubes that form the main part of the IceCube detector. Some steps of its realization are the topic of this thesis, mainly the creation of an isotropic light source from an integrating sphere made of semi-transparent PTFE on the basis of simulations with Geant4 and measurements.

Starting with a short introduction of neutrino physics and the IceCube detector this thesis will then discuss different aspects of the housing which protects the light source from its environment followed by the realization of an isotropic light source. As last step the light propagation of a POCAM pulse in the PINGU array will be simulated.

Contents

Preface

I can not begin this work without mentioning all those who did the groundwork for it. Kai Krings wrote the simulation, Joost Veenkamp and Kilian Holzapfel extended it and studied elaborately the realization of the POCAM. It was also Kilian Holzapfel who built the measuring apparatus that was used for all the measurements in this thesis and Felix Henningsen obtained and tested the hardware.

Chapter 1

Introduction

1.1 Neutrino physics

In the Standard Model of Particle Physics a neutrino is the neutral partner of an electron, muon or tauon. Since it carries neither electric charge nor color charge it does only react due to the weak interaction resulting in a very small cross section. Early neutrino detection experiments used the high neutrino flux of reactors to detect them via inverse β-decay ($\bar{\nu}_e + p \rightarrow e^+ + n$, Cowan-Reines experiment [1]), which is however not possible for the low flux we get from astrophysical or atmospherical neutrinos. Instead the deep inelastic scattering of neutrinos is used, causing the neutron on which it scatters to decay into various hadrons (hadronic shower). If the scattering happened due to W-Boson exchange, the neutrino will become a charged lepton. For energetic neutrinos the momentum transfer to the generated lepton can be big enough for the lepton to be faster than the speed of light in the medium, Cherenkov radiation appears. The Cherenkov light is emitted in a conic shape with $\cos\theta = \frac{1}{n\beta}$. From the orientation and the opening angle of the cone the energy and the direction of the neutrino can be gathered [2].

1.1.1 Neutrino mass and oscillations

Within the Standard Model neutrinos have no mass, effects such as neutrino oscillations however contradict this theory. One popular example for this case are solar neutrinos which are created in various processes in the core of the Sun. Using sun models the electron neutrino flux can be calculated, but measurements show that significantly less electron neutrinos than expected reach Earth [3, 4]. The discrepancy, which is to big to be explained by inaccurate sun models, can be explained if the eigenstates of propagation (mass) of the neutrinos are not the same as the eigenstates of the weak interaction in which they are created. If the masses are different, the neutrinos can oscillate between their flavours, the missing electron neutrinos appear as muon and tau neutrinos. The second popular example for neutrino oscillations are the oscillations of atmospheric neutrinos that change flavour on their way through Earth. Detectors such as Super-Kamiokande measure different fluxes of ν_e and ν_μ depending on the direction as a different direction means a different path length trough Earth for a neutrino created in the atmosphere on its way to the detector in Kamioka [5].

With three neutrino flavours the mass eigenstates are calculated with the Pontecorvo-

Maki-Nakagawa-Sakata matrix (PMNS matrix). A simple understanding of neutrino oscillations can be reached considering only the two flavours ν_e and ν_μ. The mass eigenstates ν_1 and ν_2 can then be calculated by a rotation matrix with mixing angle θ.

$$\begin{pmatrix} \nu_1 \\ \nu_2 \end{pmatrix} = \begin{pmatrix} \cos\theta & -\sin\theta \\ \sin\theta & \cos\theta \end{pmatrix} \begin{pmatrix} \nu_e \\ \nu_\mu \end{pmatrix} \tag{1.1}$$

The time evolution of a neutrino in natural units is given by e^{-iEt} where E is usually approximated with

$$E = \sqrt{p^2 + m^2} \approx p + \frac{m^2}{2E} \tag{1.2}$$

since the mass of neutrinos is much smaller than their momentum [5]. As they are highly relativistic particles one can also approximate $t \approx L$ with L the path length. Therefore using Einsteins sum convention the transition probability between ν_e and ν_μ is given by

$$P\left(\nu_e; 0 \to \nu_\mu; L\right) = |\langle \nu_e | \nu_i; 0\rangle \langle \nu_i; L | \nu_\mu \rangle|^2 = \sin^2(2\theta)\sin^2\left(\frac{(m_2^2 - m_1^2)\cdot L}{4E}\right) \tag{1.3}$$

The determination of the mass of the neutrinos has proven to be difficult, till this day only upper limits are known as well as the quadratic mass differences that can be gathered from the measurement of the oscillations. Not even the mass hierarchy could be determined, a hierarchy analogous to the charged leptons is possible (normal hierarchy, $m_e < m_\mu < m_\tau$) as well as the so called inverted hierarchy $m_\tau < m_e < m_\mu$ [5]. We see that a detector aiming to determine the quadratic mass difference needs a good resolution in E which motivates the construction of the Precision Optical Calibration Module.

1.1.2 Neutrino sources

The neutrinos measured on Earth can be separated in two groups. Astrophysical neutrinos are created in the universe. The mechanisms of their production have not yet been completely understood as some of the events measured in the IceCube Neutrino Observatory had energies in the range of PeV [6], the possible sources are denoted cosmic particle accelerators [5].

The second group of neutrinos are the atmospherical neutrinos created by energetic particles such as nuclei hitting the atmosphere. The particles of this cosmic radiation are mainly protons (79%) and alpha particles (15%) [7] with energies that stretch over ten orders of magnitude as can be seen in Figure 1.1.

Although particles below 10 GeV tend to be influenced by solar winds and Earths magnetic field [7] the cosmic radiation is mostly isotropic [8]. When measuring the cosmic radiation on Earth we however do not measure single cosmic rays. On their way through the atmosphere they create cascades of secondary particles, mainly hadrons, that in turn decay into charged leptons and neutrinos [5, 7]. Those air showers are distributed over large areas on the ground and motivate the construction of large area detectors such as IceTop [7, 9].

The neutrinos from air showers form the predominant part of measured events in IceCube and are divided in conventional neutrinos from pion and kaon decay and prompt neutrinos from the decay of heavier hadrons which have different yet overlapping energy spectra.

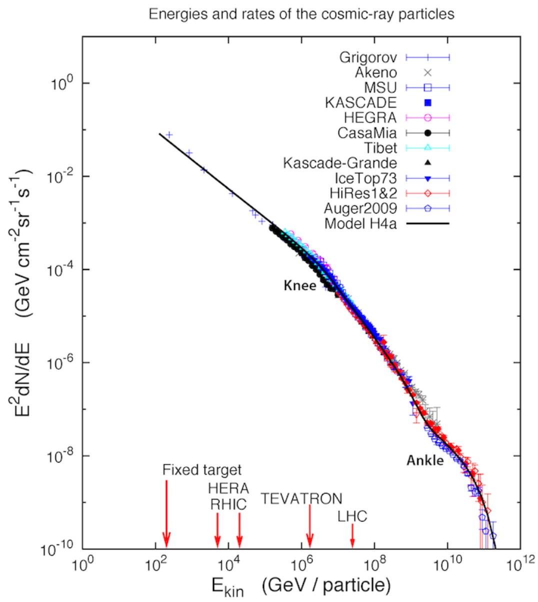

Figure 1.1: Spectrum of cosmic radiation (Source: IceCube Collaboration, retrieved from `https:/http://icecube.wisc.edu/news/view/141`)

1.1.3 Neutrino creation processes

Whereas all beta decays involve neutrinos for the IceCube detector only the processes creating solar and atmospherical neutrinos are relevant. Solar neutrinos are mainly (99.8%) produced as electron neutrinos during the fusion of protons to deuterium in the core of the Sun [10].

$$p + p \rightarrow {}^2H + e^+ + \nu_e \tag{1.4}$$

Atmospheric neutrinos are mainly created via pion decay from pions created by cosmic radiation hitting the atmosphere

$$\pi^+ \rightarrow \mu^+ + \nu_\mu \qquad \pi^- \rightarrow \mu^- + \bar{\nu}_\mu \tag{1.5}$$

The direct decay into electrons is almost negligible due to helicity suppression [10]. Since the muons can further decay we could without neutrino oscillations expect a ratio of $\nu_\mu : \nu_e = 2 : 1$.

$$\mu^+ \rightarrow e^+ + \bar{\nu}_\mu + \nu_e \qquad \mu^- \rightarrow e^- + \nu_\mu + \bar{\nu}_e \tag{1.6}$$

The decay of heavier mesons, such as kaons and D-mesons, is analogous, only the energy spectrum is different.

$$K^+ \rightarrow \mu^+ + \nu_\mu \qquad K^- \rightarrow \mu^- + \bar{\nu}_\mu \tag{1.7}$$

1.2 The IceCube Neutrino Observatory

The IceCube Neutrino Observatory is a large scale Cherenkov detector built into the Antarctic ice. Its goal is the detection of neutrinos with energies in the 100 GeV to PeV

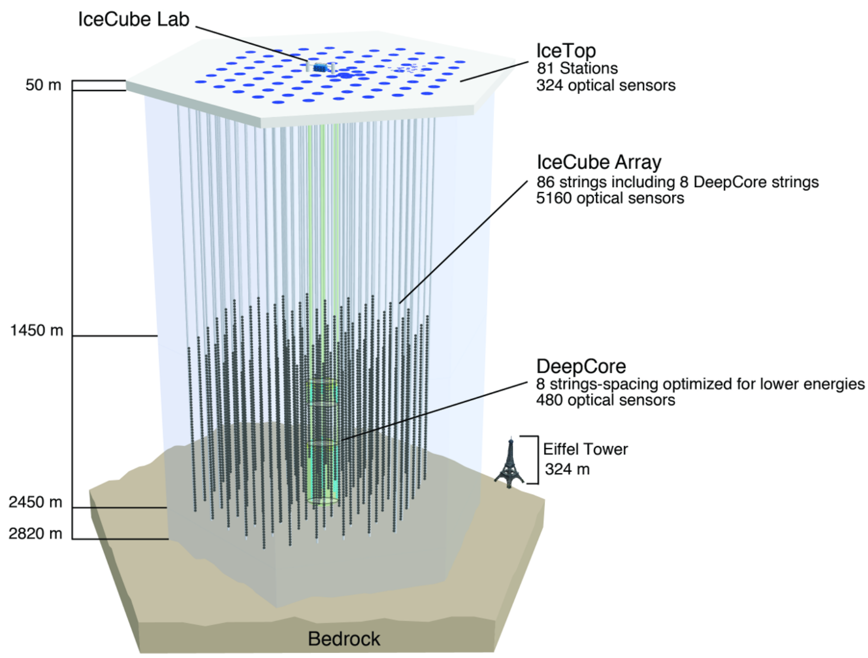

Figure 1.2: The IceCube array (Source: IceCube Collaboration, retrieved from `https://gallery.icecube.wisc.edu/internal/v/graphics/arraygraphics2011/blueTopArrayWLabels.jpg.html`)

range. 5160 Digital Optical Modules (DOMs) are placed on 86 strings in a depth of 1450 to 2450 m, the strings form a hexagonal grid with a base length of 125 m spreading the DOMs over a volume of one cubic kilometer. Each string holds 60 DOMs with a 17 m spacing [11]. The benefit of using ice in such depths is that it has almost no impurities, air bubbles vanish under the high pressure [12]. Dust however is still in the ice, due to the quite steady growth of ice the dust layers are almost homogeneous in x and y, the optical properties of the ice depend mostly on the depth z [13]. The scattering length of the glacial ice in these depths can go from 5 m in the dust layers up to 90 m for light with a wavelength of 400 nm. The absorption length is always approximately four times as big [14].

In addition to the DOMs in the deep ice multiple DOMs are placed at the surface in ice containers since the natural ice is not clear enough at low depths. This extension called IceTop serves the analysis of cosmic radiation [9].

1.2.1 The Digital Optical Module

The Digital Optical Module (DOM) as essential part of IceCube consists of a large photomultiplier inside a glass sphere. Additional parts inside the glass sphere are a mu metal grid as protection from the magnetic field of the Earth, diverse electronics and 12 LED flashers allowing testing and calibration [13]. The photomultiplier fills almost half of the sphere and is facing downwards (north) to reduce the influence of non-Cherenkov radiation coming from above. The signal gets digitized inside the DOM and sent through

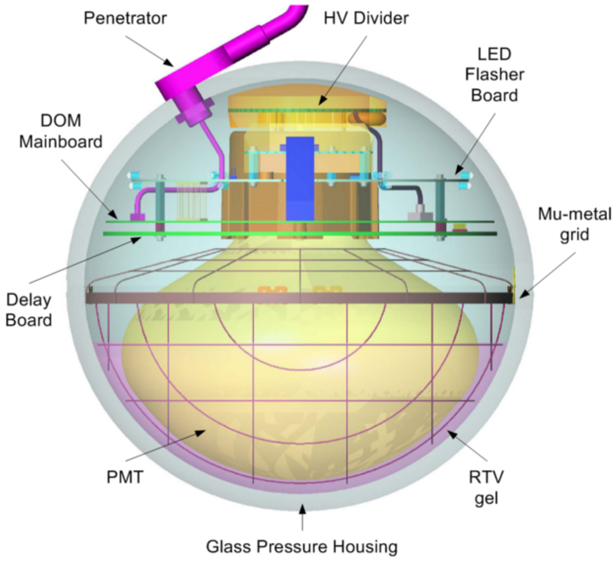

Figure 1.3: The DOM (Source: IceCube Collaboration, retrieved from `https://wiki.icecube.wisc.edu/index.php/File:DOM-Picture.png`)

the main cable of the string to the surface [15].

1.2.2 IceCube-Gen2 and PINGU

IceCube-Gen2 is a planned upgrade for IceCube, extending the detector over ten cubic kilometers. For this a wider DOM spacing has to be used which leads to a higher energy threshold. As Gen2 is designed to detect high energy astrophysical neutrinos this is not a disadvantage but leads to a reduction of the noise from atmospherical neutrinos [16].

Another planned extension is the Precision IceCube Next Generation Upgrade (PINGU) which allows the detection of lower energies and will consist of denser strings in the center of IceCube. In a depth from 2100 to 2450 those strings will bear DOMs with a spacing of 7 m. One of its goals is the determination of the neutrino mass hierarchy [17].

1.2.3 Events in IceCube

Neutrino events in IceCube are separated in two, track-like events caused by single highly relativistic muons and cascade-like events for other particles such as fast electrons that on their therefore very short path create large numbers of secondary particles who in turn can create other particles. The Cherenkov light of those particles is measured in the DOMs. The reason for muons forming tracks is their high mass (compared to the electron) and their long lifetime (relative to tauons) allowing them to travel kilometers before losing their energy [16].

1.2.4 Deployment

Of particular interest to us is the deployment of the IceCube DOMs, as it shows some requirements the POCAM has to fulfill. A hole is molten into the ice and the DOMs are lowered into it on the strings, afterwards the hole freezes again. In depths of 2 km and more the water pressure alone is more than 200 bar. When it comes to expansion during the freezing process even higher pressure will be reached, the POCAM should therefore resist at least 1000 bar. Additionally the refrozen ice is of lower clarity, air bubbles are frequent and tend to concentrate on the center of the drill hole.

Chapter 2

POCAM introduction and overview

The purpose of the Precision Optical Calibration Module (POCAM) is the calibration of the low energy scale of PINGU. Where the DOM practically is a photomultiplier tube the POCAM is a light source. Just like a DOM it will be deployed on a string in the deep glacial ice.

2.1 The goal of isotropy

Since it is hardly possible to control the exact orientation of the POCAM after its deployment it would be difficult to compensate for dependencies of the light intensity from the angle. Therefore the primary goal of the POCAM has to be isotropy. An absolute isotropy in 4π is not possible, the power cable will cast a shadow and so do control electronics and parts of the mechanical construction. It has to be ensured that the shadows cast by those objects can be easily cut out of the later calibration methods. The shadows should therefore be not smeared out, few large shadows are preferred over many small ones. It also has to be ensured that these objects do not disturb the light output of the POCAM by reflecting light.

2.2 The integrating sphere

To achieve isotropic light output a sphere made out of thin PTFE is used. PTFE reflects light with a cosine distribution (Lambertian). In the thickness of few millimeters a significant part of the light is transmitted. Due to repeated reflection the light emitted from a light source inside the sphere will become almost completely isotropic. The original idea for the integrating sphere was a non transmitting sphere with small holes in it allowing the light to leave the sphere. This construction is also known as Ulbricht sphere and is commonly used in spectrometry. The semi-transparent PTFE sphere is the limit of this construction with infinitely many infinitely small holes.

2.3 Light pulses

To enable calibration not only by intensity but also by time the POCAM is not a constant light source but will emit short flashes of some nanoseconds. The light source, a LED with a wavelength in the area of $380 - 430$ nm, is powered by a Kapustinsky circuit creating a very short pulse. The wavelength is chosen with respect to the DOM photomultiplier tubes which are the most sensitive in this area [18].

2.4 Construction

Like the DOM the POCAM needs a housing to protect it from ice and pressure. As a test setup with a smaller drill hole is likely, the POCAM will not simply use the same housing as the DOMs do. Instead a glass sphere of a 57 mm radius and a 7 mm thickness is used. The sphere consists of two hemispheres, one of them contains a vacuum plug and a plug with a connector to a data cable and is made out of optical BK7 glass with a low absorption coefficient. The sphere is already manufactured, the outer dimensions of the POCAM are therefore fixed. The two glass hemispheres are held together by a waistband, which will be also used to mount the POCAM to the string. Since electronics and plugs will cast large shadows, an isotropic light source illuminating 4π is not possible. Therefore only one hemisphere of the POCAM will be optimized as isotropic light source in 2π, the other hemisphere containing the plugs will be darkened. Two POCAMs will in the final setup illuminate 4π.

The size of the integrating sphere is determined by the POCAMs outer dimensions. If any electronics should fit in the housing, whose space is already limited by the plugs, the integrating sphere can not be bigger than $r = 25$ mm. Any smaller radius will greatly limit the possibilities for mounting it, therefore $r = 25$ mm is the size of choice.

2.5 Simulation details

For all following simulations some general values will be used and are briefly discussed here.

Wavelength

The wavelength which depending on the LED finally used will lie somewhere between $380 - 430$ nm as the photomultiplier tube of the DOMs is the most effective in this area [18]. In the simulations it is set to 405 nm. One can assume that changes of refractive indices and absorption coefficients are small in this area [19].

Ice and hole ice

The optical properties of glacial ice and the refrozen ice of the drilling hole differ significantly. The glacial ice has scattering lengths of about 50 m [12, 14] whereas the hole ice has a significantly lower scattering length (≈ 50 cm [20]) due to its many air bubbles. We will however not make this part of the basic POCAM simulation as it is already part of elaborate simulation models for light propagation through ice developed by the IceCube Collaboration. These simulations will for later calibration use the output of the POCAM simulation as input, an example can be found in Chapter 8. In the simulations of other chapters the only effect of the ice is the scattering at the POCAMs surface due to the refractive index of the ice of $R_I = 1.318$ [19].

Glass

The BK7 glass has for a wavelength of 405 nm a refractive index of $R_I = 1.53$ and an absorption length of 3.3 m [21].

Optical gel

The optical gel that is used in some simulations has a refractive index of 1.4 and an absorption length of 29 cm for $\lambda = 405$ nm as measured by Felix Henningsen of the TUM ECP group.

Other components

To reduce unwanted reflections in the final setup all non transparent components such as electronics, plugs, cables, waistband and the hanging assembly for attaching the POCAM to the string will be either black or covered by a black material. Their reflectivity is zero in all simulations.

Chapter 3

Preliminaries

3.1 PTFE

PTFE (Polytetrafluorethylene, known under the brand name Teflon) has a number of interesting chemical and physical properties such as inertness to most solvents, a very low friction coefficient and a very hydrophobic surface. For our purposes a property of thin PTFE layers is of importance. Whereas many surfaces enable Lambertian reflection, PTFE also shows a Lambertian behaviour in transmission. If the PTFE is thin enough to transmit light, the transmitted light has a cosine shape $I(\theta) \propto \cos\theta$ where θ is the angle to the surface normal.

3.2 Reflectivity and transmittance

Usually reflectivity R is defined as the ratio of the intensities of the reflected beam and the source beam for reflection at 0° to the normal, whereas transmittance T is defined as the ratio between the transmitted beam and the source beam also at 0° to the normal. Since reflection and transmission for PTFE are both Lambertian, focusing only on the normal is of limited use. When in the following paper the term reflectivity is used, it refers to the total amount of light reflected in any backwards direction relative to the source intensity, where only the source beam is parallel to the normal. The same applies to the term transmittance. Expressed in formulae for a source beam pointing towards $\theta = 0°$:

$$R = \frac{1}{I_{source}} \int_{\theta=\pi/2}^{\theta=\pi} I d\Omega \tag{3.1}$$

$$T = \frac{1}{I_{source}} \int_{\theta=0}^{\theta=\pi/2} I d\Omega \tag{3.2}$$

The absorption A is simply defined as $A = 1 - T - R$

3.3 Concept of the integrating sphere

Using the discussed properties of PTFE an isotropic light source can be imagined. The idea is to place an anisotropic light source (a LED) in a PTFE sphere (the integrating sphere) with high reflectivity and low transmittance. Repeated reflection should result in almost random photon directions and therefore in an isotropic light emission of the integrating sphere.

3.4 Geant4

All simulations were based on Geant4, a framework developed by CERN for Monte Carlo simulations of particles interacting with matter [22]. While being able to simulate various types of radiation Geant4 needs some additions to simulate PTFE. A modification by Kai Krings and Kilian Holzapfel of the TUM ECP group allowing diffuse (Lambertian) transmission is used since this effect which is the very reason why PTFE is used for the integrating sphere is no part of the repertoire of Geant4. The modification uses the in-built Lambertian refraction, but switches the sign of the vector component of the photon direction perpendicular to the surface on which the reflection happens.

Internally the Lambertian refraction in Geant4 happens on the surface only. The Lambertian transmission is therefore also limited to the surface and does not happen within the PTFE. The integrating sphere has an outer and an inner surface, giving both the property of Lambertian refraction and transmission leads to photons being reflected many times between those two surfaces. To avoid this we will reduce the PTFE effectively to a single surface, namely the inner surface of the integrating sphere.

Since these modifications overwrite the default behaviour of light in PTFE, the Geant4 simulations need to be carefully compared with measurements (Chapter 5).

3.5 The measuring apparatus

In order to compare the simulated results with data a measuring apparatus was constructed. The apparatus allows rotation in θ and ϕ for the object to be measured. The apparatus is placed in a metal box excluding external light together with a light sensor. While it is planned to later use a micro photomultiplier tube we will use a photo diode for our measurements, as the voltage drop of a photo diode in a short-circuit is linearly dependent of the light intensity. One has to consider that under certain angles the apparatus casts a shadow on the photo diode. The measured points lying in this shadow are removed from the plots since they do not contain valid data about the measured object.

In all plots of measured data error bars are given which represent the electronic noise of the photo diode and its readout electronic. In many cases repeated measurements were done to reduce the noise. Since the relative impact of the noise depends on the absolute brightness which in most plots is not visible due to normalization the size of the error can vary significantly.

3.6 Plots

When in the following chapters the dependence of the intensity on θ is of concern, one has to consider that the area of a surface segment of a sphere scales with $\sin\theta$. To

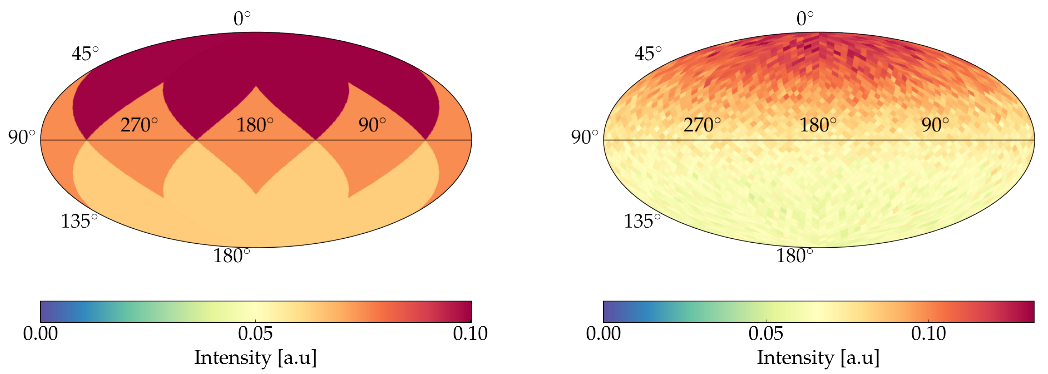

Figure 3.1: HEALPix example plots of the same data for orders 0 and 4

compensate for this the value of the bins in the histograms is divided by $\sin\theta$ which however leads to strong deviations near $\theta = 0°$ and $\theta = 90°$.

As in many cases the shape of the theta dependence is of concern and not the absolute intensity many plots are normalized in such a way that either the maximum or the mean is set to one. This allows for easier comparison between the plots.

In all visualizations of the simulated setup and in all HEALPix plots the upward direction corresponds to $\theta = 0°$.

3.6.1 HEALPix

Whenever in the following paper the angular distribution of the photons emitted from the POCAM is visualized depending on θ and ϕ, the HEALPix pixelization is used. HEALPix allows the pixelization of a sphere in pixels of equal area which are placed on lines of constant θ [23]. The pixelization allows different orders n with a total number of pixels of $12 \cdot 4^n$. The pixelated sphere surface is plotted in 2D using the Mellowed projection.

In most cases the plots use the same color scale and are normalized in such a way that the integral over the entire sphere equals one. Example plots are shown in Figure 3.1.

3.7 Notation

It is common to denote the refractive index with n. However, in this paper the number of simulated photons will be denoted by n, for the refractive index R_I is used.

Chapter 4

The light source

The POCAM will be illuminated by an LED of a wavelength of 405 nm (Sec. 2.5) powered by a Kapustinsky circuit.

4.1 Kapustinsky circuit

In order to create a very short pulse of light a so called Kapustinsky circuit is used, an easy to produce, reliable pulse generator with pulse lengths of a few nanoseconds [24][25]. To get a short overview its function is described using the time values from Kapustinsky's original paper [25].

In the Kapustinsky circuit a trigger signal with a width of 150 ns charges a capacitor. Through a high-pass filter the trailing edge of the trigger signal switches a thyristor that discharges the capacitor through a LED. An inductance parallel to the LED builds up its magnetic field, when the voltage drops during the capacitor discharge the inductance creates an opposing voltage. This reduces the long exponential decay of the capacitor from 100 ns to 12.5 ns creating a very short light pulse from the LED.

Figure 4.1 shows Kapustinsky's original circuit diagram. The thyristor is composed of two transistors.

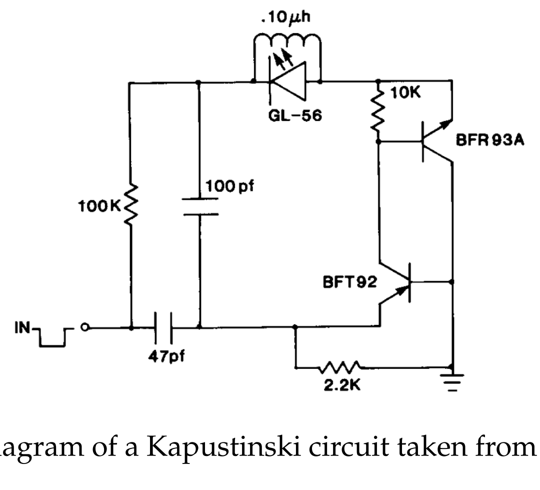

Figure 4.1: Circuit diagram of a Kapustinski circuit taken from the original paper [25]

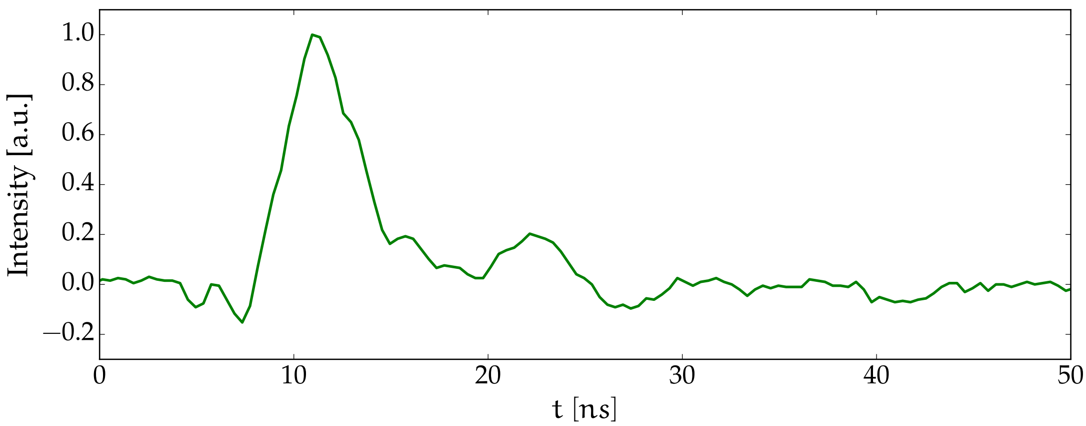

Figure 4.2: Example for the time profile of a LED in a Kapustinsky circuit measured with a pin diode as photo sensor. Measurements by Antonio Becerra Esteban of the TUM ECP group.

For the simulation only the time profile of the LED is of concern (Fig. 4.2). In order to optimize the time profile heavy testing is still in progress. This is of no concern to the simulations, as we will later see that the final time profile of the POCAM for an arbitrary LED time profile can easily be obtained without the need of a modified simulation (Sec. 7.8).

4.2 Angular intensity of LEDs

For an isotropic integrating sphere a LED with a wide opening angle is the best choice. This can be easily understood considering that the isotropy is mainly based on Lambertian reflection. However, a small quantity of the light leaves the integrating sphere without being reflected first. This results in bright spot at the outside of the integrating sphere. Even with the Lambertian transmission this effect can not be compensated. It is therefore important to come as close to isotropy as possible with the light source, a LED with a large opening angle has to be used (Sec. 7.3.1).

The LED will be used in a Kapustinsky circuit which highly depends on the inductance of the LED. Therefore the choice of the LED is not free and the usage LEDs specialized on a large opening angle becomes unlikely. We will consider only the most common types of LEDs.

Common LEDs come in two forms, one with a rounded head and one with a flat head. Figure 4.3 shows the measured angular intensity of a LED with a flat head on the example of a green SMD LED.

When testing the optical properties of PTFE such as reflectivity and transmittance we will use a LED with a small opening angle to reduce the direct light hitting the light sensor, therefore a LED with a rounded top is used. Since this LED emits some part of its light at high angles, some even to $\theta > 90°$, the LED is mounted on the measuring apparatus inside of a small tube limiting side emission and leading to an opening angle of 15° as shown in Figure 4.4.

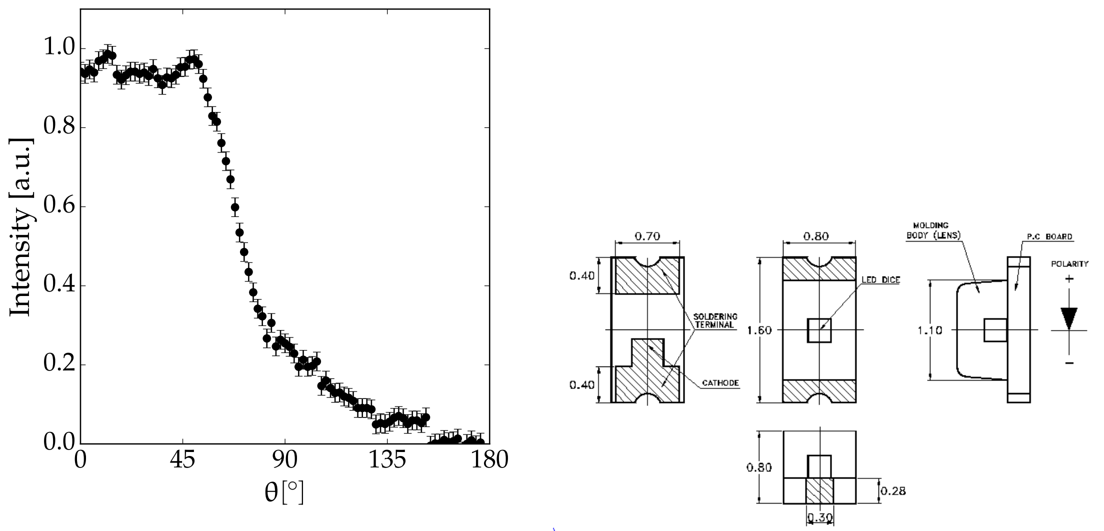

Figure 4.3: Angular intensity of a flat head SMD LED and dimensions in millimeters from from the manufacturers specifications [26]. When soldered on a board the emission for $\theta > 90°$ will vanish.

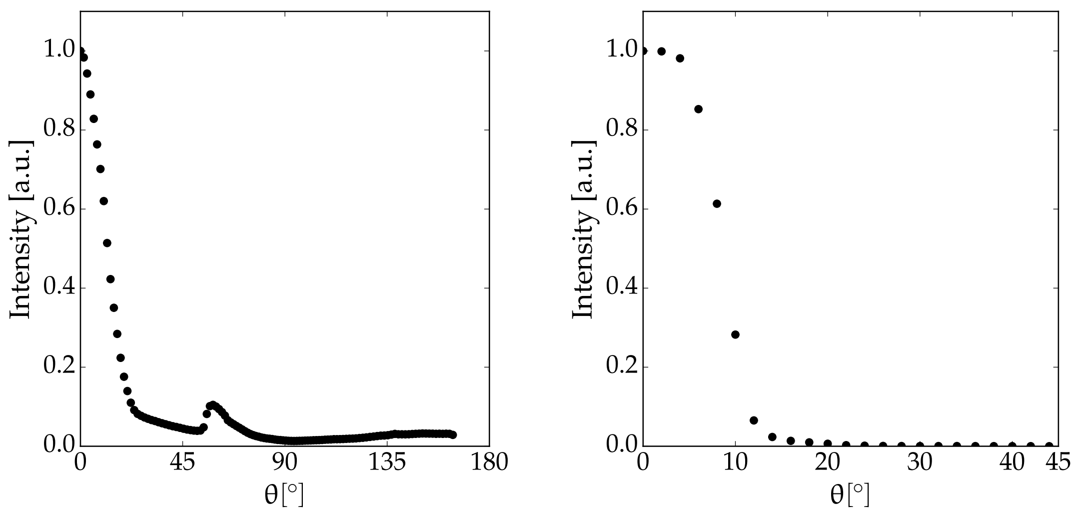

Figure 4.4: Round top LED without and with mounting limiting side emission and leading to an opening angle of 15°.

Chapter 5

Testing the validity of the simulation

In order to check the validity of the simulation we are simulating and measuring a prototype of the integrating sphere produced by the TUM workshop. This prototype has an outer radius of 60 mm and a thickness of 2 mm.

5.1 Lambertian behaviour

To determine reflectivity and transmission of 2 mm thick PTFE we will measure a plane piece of of the same PTFE that the prototype integrating sphere is made out of. The PTFE is illuminated by the LED with an opening angle of 15° from Fig. 4.4 and the measurement is done in theta for 360°. If reflection and transmission are Lambertian as expected, one can fit two cosines in the curve as shown in Figure 5.1.

Of additional interest is the question whether the Lambertian transmission depends on the angle of the LED to the PTFE. Figure 5.2 shows the angular intensity for the angles 0°, 24° and 43° to the normal. The good fit of the cosine function as well as the same intensity for each measurement show accordance with the expected behavior.

5.2 Simulating plane PTFE

Ignoring the absorption ($T + R = 1$) in the PTFE we get from the fits in Figure 5.1 a ratio of transmittance to reflectivity $T/R = 0.2691$ and therefore $T = 0.212$ and $R = 0.788$. A simulation of 2 mm plane PTFE is shown in Figure 5.3. We see that the modifications of Geant4 have the expected effect.

5.3 Measurement of the integrating sphere prototype

We now come to the measurement of the integrating sphere prototype. While in principle for an isotropic integrating sphere we would use a flat head LED, we will now use the LED with an opening angle of 15° we used before. The goal is to have an anisotropic output in order to compare the measured and simulated anisotropy.

The LED was placed at a distance of 7 mm from the center pointing towards the center. The sphere has an outer radius of 30 mm and a thickness of 2 mm.

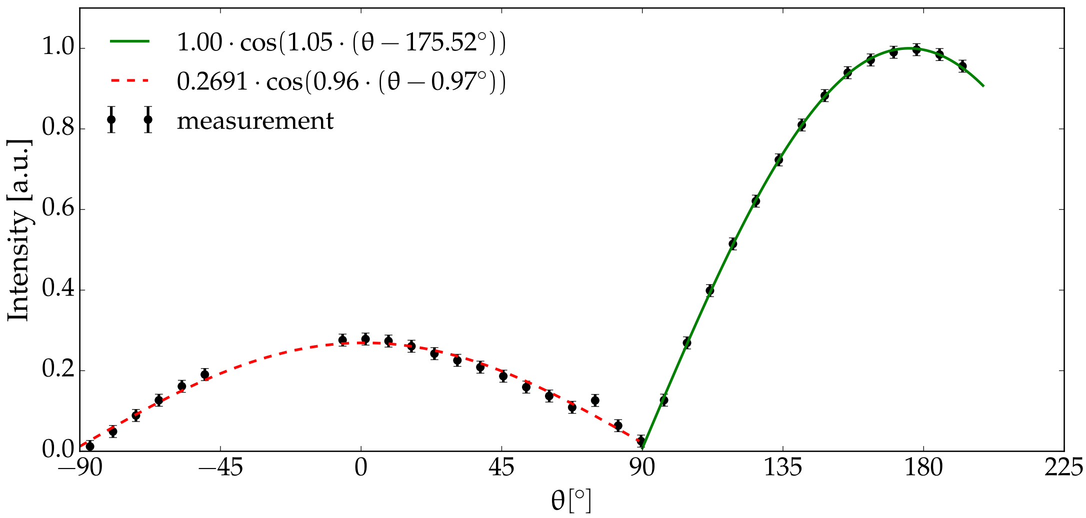

Figure 5.1: Lambertian reflection ($\theta > 90°$) and transmission ($\theta < 90°$) on plane PTFE. The maximum of the cosine fit for the reflection was arbitrarily set to one.

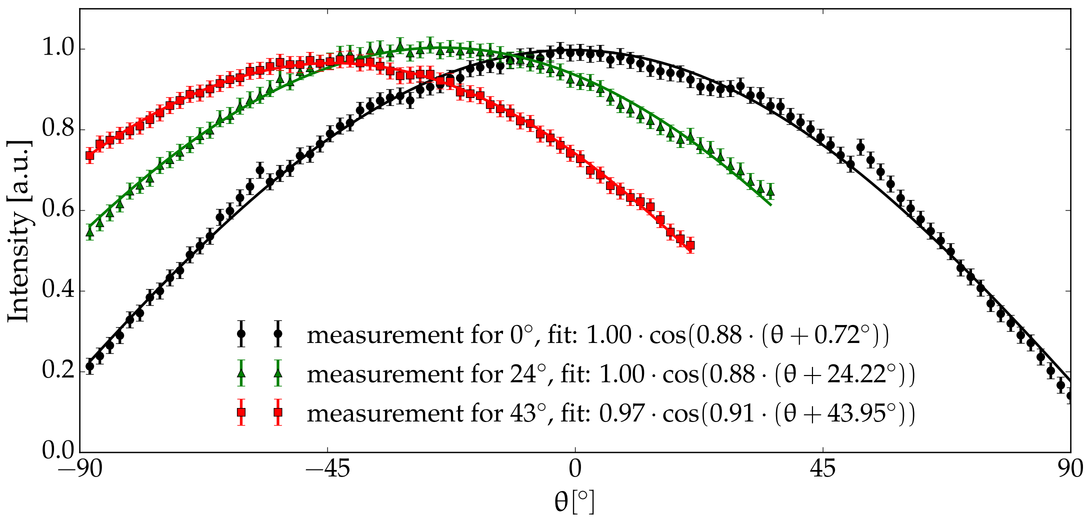

Figure 5.2: Lambertian transmission for different angles of the LED to the normal of the PTFE surface. Normalized by setting the maximum of the cosine fit for 0° to 1.

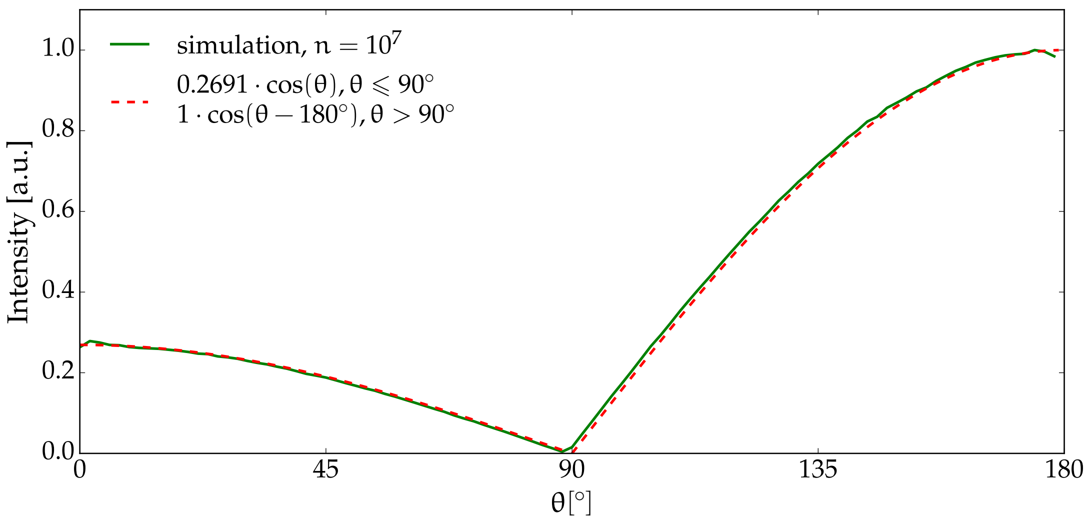

Figure 5.3: Simulation of plane PTFE and theoretically expected curve

Figure 5.4 shows the measurement of the integrating sphere prototype. One clearly sees the bad integrating properties due to the high transmission coefficient of the PTFE. The high transmission allows for a significant part of the light of the LED to pass through the PTFE without being reflected. This results in a bright spot on the integrating sphere on the side opposite to the LED which has a cosine-shaped impact on the angular distribution.

5.4 Simulating the integrating sphere prototype

Using the reflection and transmission coefficients gathered from the measurements with the plane PTFE we can simulate the integrating sphere. The LED with the 15° opening angle was simulated using an intensity parametrization of

$$I(\theta) = 0.5 + 0.5 \cdot \cos(\theta/15° \cdot 180°)\,, \quad \theta \in [0°, 15°[\tag{5.1}$$

In later simulations the direction of the photons will be plotted which corresponds to the light intensity on a spherical surface encompassing the setup at $r = \infty$. Since we can not measure at $r = \infty$ in this particular simulation a modification was made to measure the intensity of the light at a radius of 30 cm from the center of the sphere in addition to the intensity at $r = \infty$ where 30 cm was the distance of the photo diode to the center of the sphere in the measurement. Plots for both distances are shown in Figure 5.5 where the quite significant difference between the two is visible. For comparison the measured values are also plotted as is the original angular distribution of the simulated LED. One sees that simulation and measurement agree with each other with small deviations attributable to the neglected absorption. Future simulations can therefore be considered good approximations to the expected measured data.

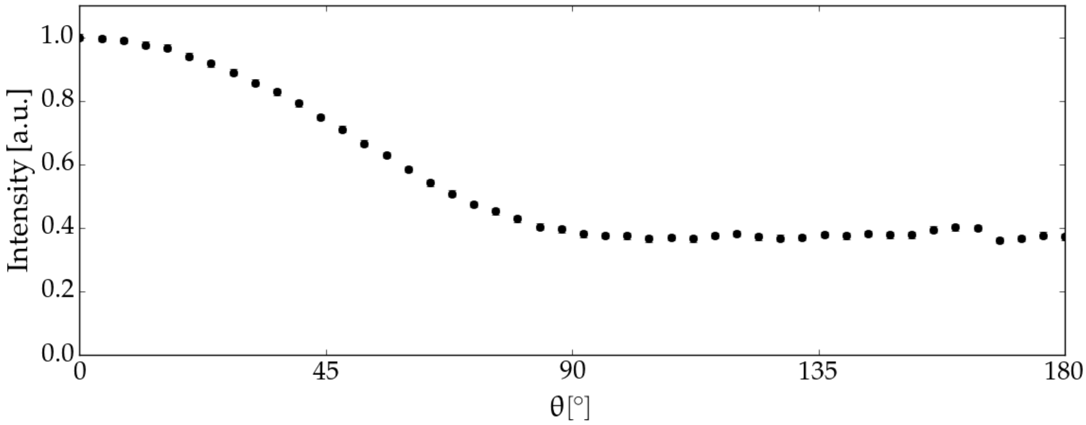

Figure 5.4: Measurements of the integrating sphere prototype

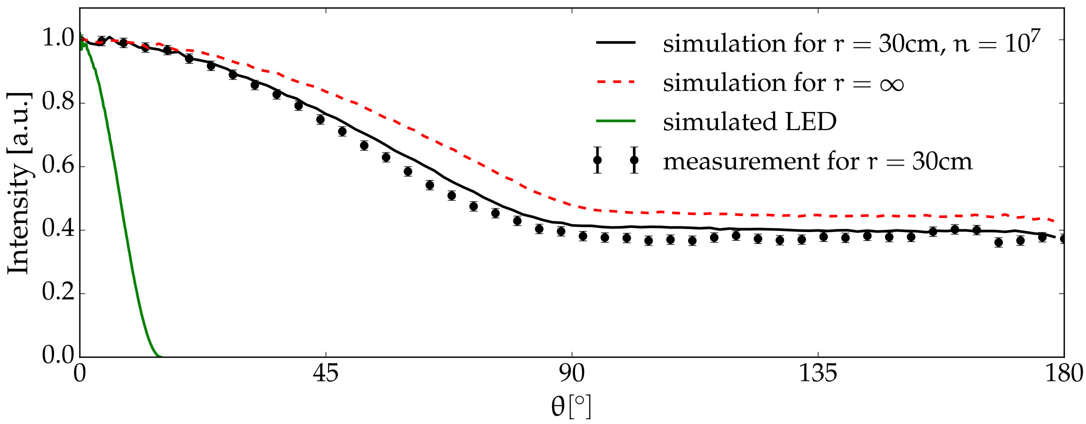

Figure 5.5: Simulation of the integrating sphere prototype. All curves normalized to 1 at $\theta = 0°$.

Chapter 6

Housing sphere

The POCAM needs some sort of housing to protect it from external influences. The housing will be made out of glass, more specifically BK7 glass with high pressure resistance and low absorption. Inside the housing we need the integrating sphere, the Kapustinsky circuit and other electronics, a microcontroller to communicate with the outside and a micro photo multiplier tube for testing. Additionally the housing needs a port for a data cable and a vacuum port, which will be used to evacuate the housing in order to fill it with optical gel or a protective atmosphere. A picture of the lower hemisphere can be found in Fig. 6.1.

6.1 Setup

The integrating sphere is placed inside a glass sphere consisting of two halves. The holes for the plugs are both on one hemisphere. As sealing an isolating band, the waistband, surrounds the equator.

The vacuum plug and the data cable already cast huge shadows as do the electronics to control the LED and the waistband. Since complete isotropy in 4π is therefore not possible, the most likely configuration has a darkened lower half. The benefit of this configuration is one clear shadow which can be cut out of later calibration methods. This way two POCAMs are needed to illuminate 4π. Figure 6.2 shows a visualization, whereas Figure 6.3 shows a true to scale sketch. The illuminated hemisphere points up ($\theta \leqslant 90°$) in all following sketches and simulations. This does not need to correspond with the final orientation of the POCAM in the ice.

6.2 Optical gel and integrating sphere offset

In order to strengthen the housing mechanically it could be filled with optical gel. The available gel has a refractive index of 1.4 and an absorption length of 290 mm for a 405 nm wavelength. Of special interest are the shape of the shadows and the total light output of a POCAM with and without optical gel.

To study these effects independent of possible anisotropies of the integrating sphere we will run the simulation with an idealized integrating sphere of absolute isotropy.

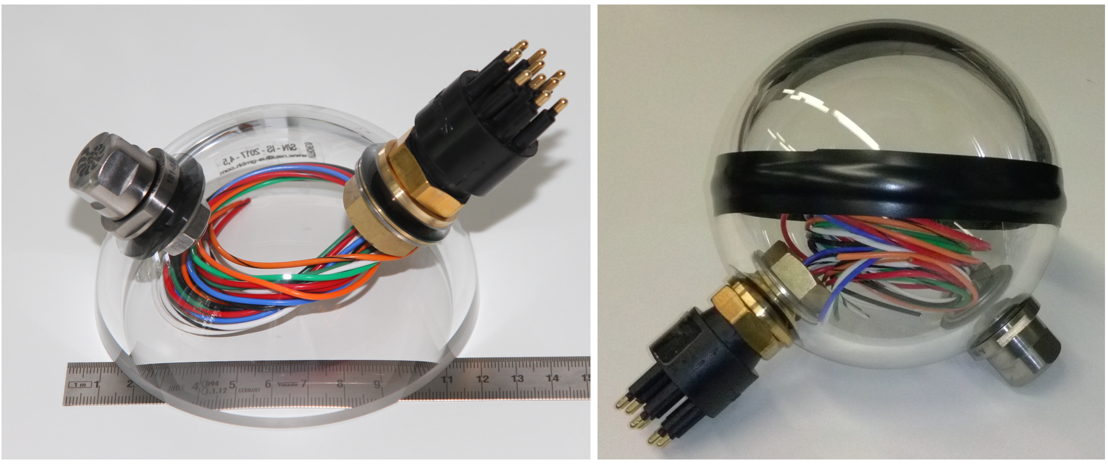

Figure 6.1: Left: photo of the lower housing hemisphere, photographed by Felix Henningsen of the TUM ECP group. Right: the housing with waistband.

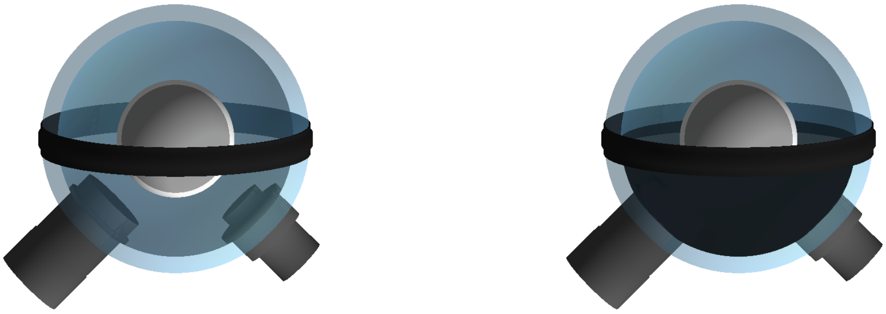

Figure 6.2: Visualization of the POCAM with housing, waistband and plugs, without and with blackened hemisphere

6.2.1 Total light output

Since the optical gel has a refractive index of 1.4 which is close to the refractive index of the housing glass of 1.53 one can expect the reflection between gel and glass to drop. A simulation shows that the average number of reflections on the glass per photon is 5% without and 0.8% with gel. This however does not compensate for the absorption by the gel, the total amount of photons leaving the POCAM with the gel is only 91% of the number leaving it when no gel is used, as one would expect given the short absorption length.

All following simulations show the the same ratio of total light emitted between configurations with and without gel. Therefore in future plots only the shape of the angular distribution of the intensities will be of concern, not the absolute magnitude. To enable easier comparison the difference in absolute light will be compensated by normalization.

6.2.2 Shadows

As the optical gel changes the angle of the photons entering the glass, the shape of the shadows cast by the waistband and the plugs could change. To test this we simulate

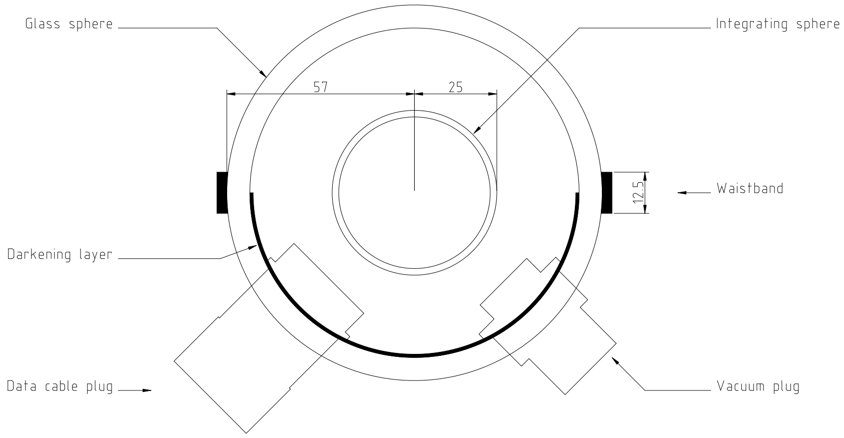

Figure 6.3: True to scale sketch of the POCAM with blackened hemisphere. All lengths in mm.

the glass sphere with waistbands of different widths (Fig. 6.4). We see that the optical gel smears out the shadow.

The effect can be simply explained. A point on the inside of the glass is hit by photons with a maximal angle of θ_{in} depending on distance and size of the integrating sphere. According to Snell's law the photon changes its angle to θ_{Glass} with

$$n_{in} \sin\theta_{in} = n_{Glass} \sin\theta_{Glass} \tag{6.1}$$

The same applies upon leaving the glass, solving for the angle θ_{out} yields if we neglect the curvature of the glass

$$\theta_{out} = \sin^{-1}\left(\frac{n_{in}}{n_{out}} \sin\theta_{in}\right) \tag{6.2}$$

One sees that with increased inner refractive index each point of the outside emits light with a wider angle. Therefore the borders of shadows are smeared out.

We can also simulate the POCAM with waistband and plugs as shown in Figure 6.5. The same effect is visible.

6.2.3 Offset

To allow more electronics to fit in the POCAM we will consider placing the integrating sphere with an offset to one side. A problem with this configuration is that the housing could act as a lens and destroy the initial isotropy of the integrating sphere. We will simulate the POCAM for two offsets with and without optical gel but also with and without waistband as to separately examine the effect on the isotropy and the effect on the shape

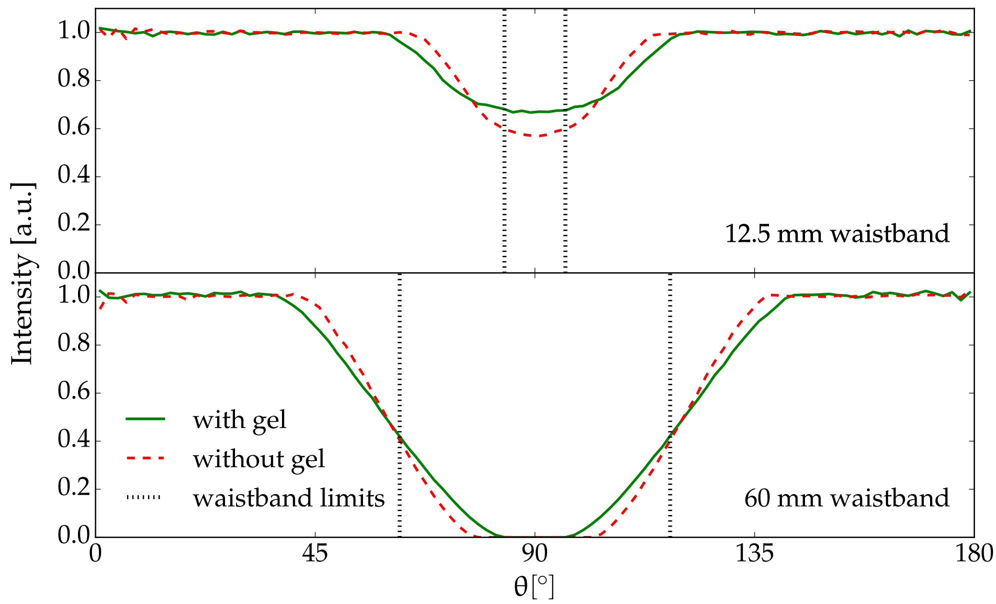

Figure 6.4: Smearing of the shadow due to the optical gel for two waistband sizes

of the shadows. A visualization of the simulated configurations is shown in Figure 6.6. Figure 6.7 shows clearly that an offset distorts the isotropy and is not desirable. Since the optical gel limits this effect, we might consider using optical gel to compensate for small dislocations of the integrating sphere caused by external force or deformation due to thermal contraction. An additional simulation is made with an offset of 1 mm and shown in Figure 6.8. One sees that if isotropy to a precision of less than one percent is needed, the optical gel can be quite useful.

6.2.4 Conclusive remarks

The previous section has shown no overall advantage of either configuration, the preference depends highly on mechanical limitations. If a precise and stable mounting of the integrating sphere can be reached, optical gel should not be used, if not, it should be used at the cost of large penumbrae.

6.3 Main board

While the final electronics configuration is still under consideration, the dimensions of the main circuit board can already by gathered. The main board needs to sit below the integrating sphere on the side containing the plugs. This results in a circular board with two openings. Based on the dimensions of the sphere a simple cardboard model was made and inserted as a test. A sketch can be found in Figure 6.9. The board shows sufficient size for the placing of multiple Kapustinsky circuits which would allow to place multiple LEDs with different properties in the POCAM.

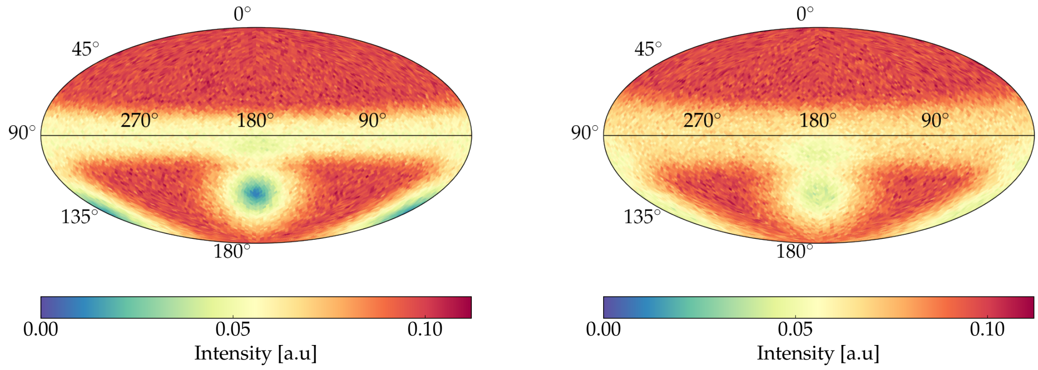

Figure 6.5: Simulated angular dependence of the intensity for an integrating sphere with waistband, vacuum port and data cable plug simulated without (left) and with optical gel (right). In this simulation the lower hemisphere is not darkened. The simulations were done with $n = 10^7$ photons

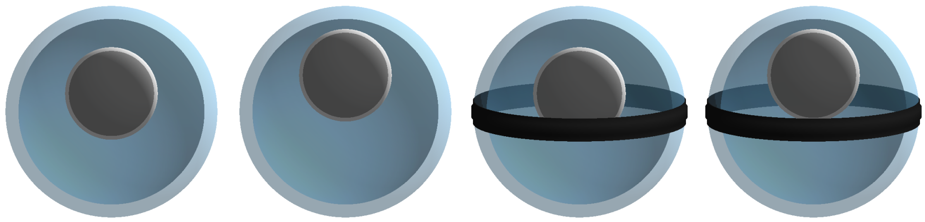

Figure 6.6: The different configurations to be simulated

6.4 Data cable and hanging assembly

Finally we have to consider the POCAMs connection to the outside world. A data cable will lead from the designated plug to a larger main cable. This cable will most likely not end at the POCAM but continue to greater depths either to DOMs in the final setup or to other measuring devices in test setups.

Additionally some sort of hanging is needed. While the final shape heavily depends on the respective deployment some cases should be considered in advance.

One possibility could be a reusing of the DOM hanging. The suggested setup is an aluminium waistband surrounding the sealing waistband. From the aluminium waistband three cables each lead upwards and downwards joining in a hook connected to the main cable (Fig. 6.10). To minimize shadows these hanging cables should have some distance to the POCAM and the orientation should be chosen in such a way that the shadow of one of this cables superposes the shadow of the main cable.

The simulations in Figure 6.11 show the angular intensity distribution of such a setup. Hanging cables with a diameter of 4 mm were used. The main cable has a diameter of 36 mm [17].

Unfortunately the shadows of the hanging cables cover a large part of the upper hemisphere. A better solution would be to have only one cable leading upwards. This cable

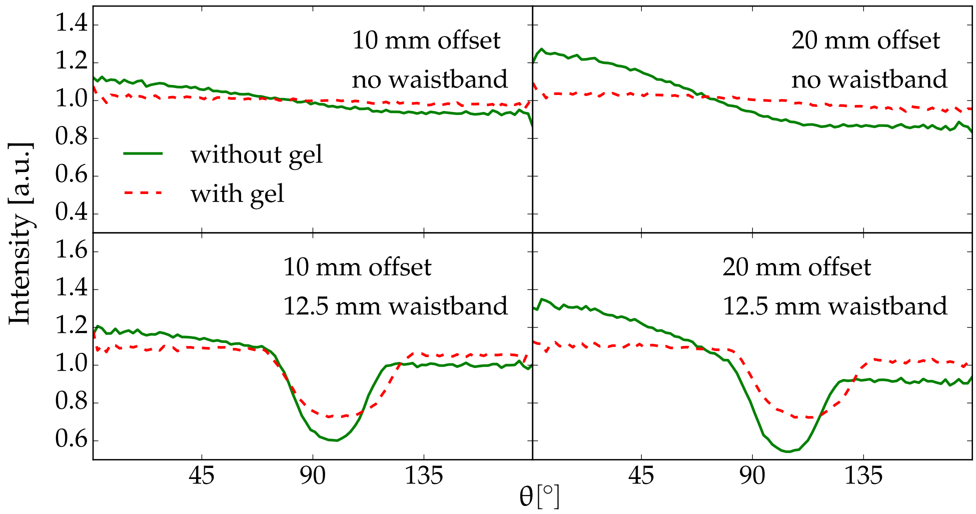

Figure 6.7: Simulation of the different configurations with $n = 5 \cdot 10^6$ photons, the mean of each plot is normalized to 1

needs to sit above the center of mass, therefore a solid arc of aluminium leads upwards from the waistband to join with the cable (Fig. 6.12). If necessary the waistband can be enforced on the dark hemisphere. If the aluminium arc is arranged in such a way that the shadow it casts lies in the same direction as the shadow of the waistband, eventually enforced by additional cables between the two, much better results can be obtained (Fig. 6.13).

Variations of this concept are possible. For a more flexible main cable for example the arc could follow the curvature of the main cable and both could be joined together.

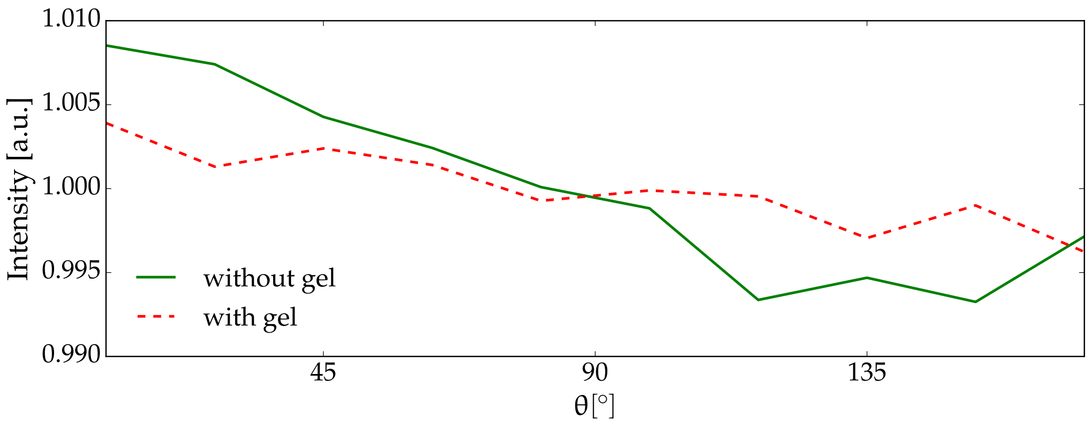

Figure 6.8: Simulation for a very small offset of 1 mm without waistband with $n = 10^7$. Due to the smallness of the effect the histogram has only 10 bins to smoothen statistical noise.

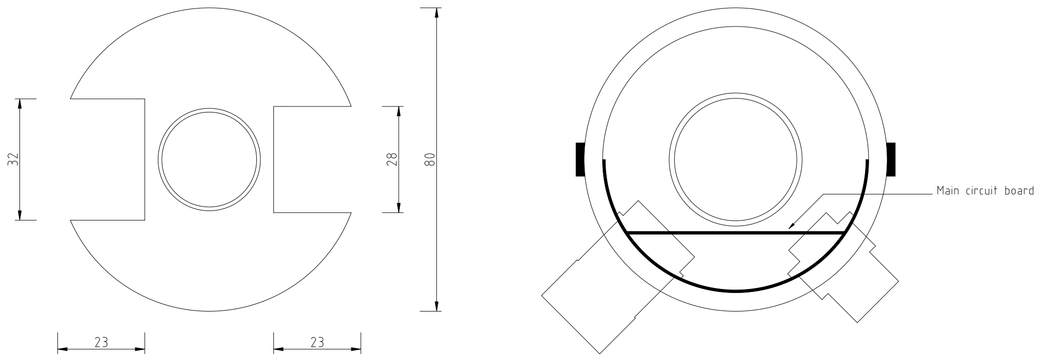

Figure 6.9: Dimensions and position of the main circuit board. All dimensions in millimeter.

Figure 6.10: Left: Sketch of the DOM hanging. (Source: IceCube Collaboration, retrieved from `https://wiki.icecube.wisc.edu/index.php/File:DOM_illust_color_big.jpg`) Right: Suggested similar hanging for the POCAM.

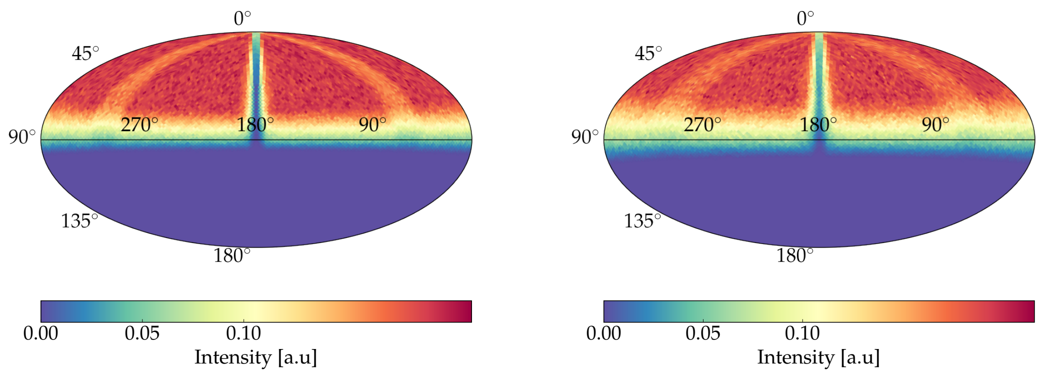

Figure 6.11: Simulation of $n = 10^7$ photons for a POCAM with DOM-like hanging without (left) and with optical gel (right).

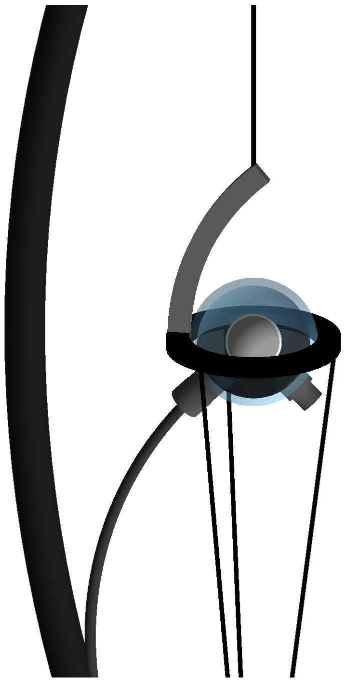

Figure 6.12: Visualization of the aluminium arc hanging. For identification the aluminium arc is colored in gray.

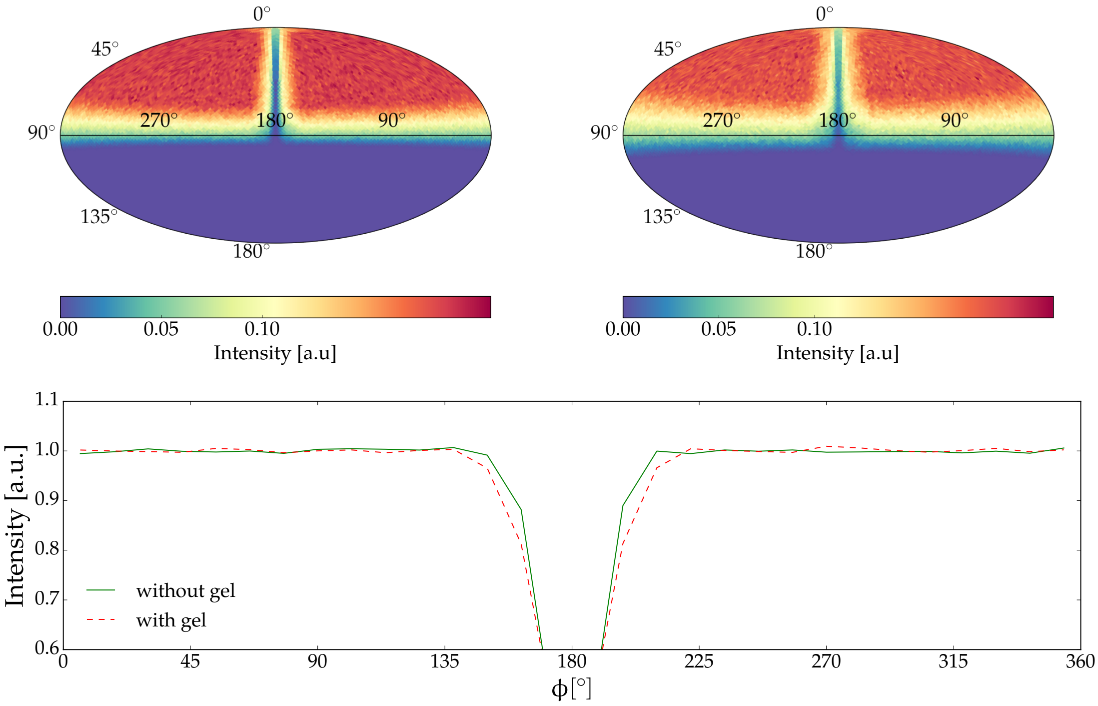

Figure 6.13: Simulation of $n = 10^7$ photons for the setup visualized in Figure 6.12 without (top left) and with optical gel (top right). The lower graph shows the dependence on ϕ for $20° \leqslant \theta \leqslant 70°$.

Chapter 7

The integrating sphere

We will now consider the properties of the integrating sphere. At first we will try to gather some information over the influence of certain parameters on the isotropy. Based on this concrete specifications for the construction will be made. Towards the end of the chapter some actual constructions will be measured and discussed using the prototype and spheres obtained from a manufacturer of ball bearings.

Please note that in this chapter the light source in most cases points towards $\theta = 0°$. The transparent hemisphere of the housing is supposed to go from $\theta = 0°$ to $\theta = 90°$.

The simulated integrating spheres in this chapter are practically the already mentioned prototype integrating sphere ($R = 0.79$, $T = 0.21$) as we know that a sphere with such properties can be produced. The radius is changed to 25 mm to allow more electronics to fit into the POCAM.

7.1 Contributing surface

Every point on the surface of the integrating sphere can only emit light at maximally 90° to the normal. A simple sketch (Fig. 7.1) can show which area of the integrating sphere does not contribute to the illuminated upper hemisphere. We see that a rather large part of the integrating sphere can be accessed from the outside for inserting the LED, even multiple LEDs are possible, and mounting it to the housing. Please note that this only concerns objects on the outside of the integrating sphere. Objects on the inside are discussed in Section 7.4. This also explains why no radius smaller than 25 mm should be used, since this would result not only in less usable surface per solid angle but also in a smaller solid angle.

7.2 Causes of anisotropy

In order to create an isotropic integrating sphere a basic understanding of possible anisotropies is necessary. The assumption is that almost the entire anisotropy is created by photons leaving the integrating sphere without ever being reflected. After the first reflection, perfect isotropy is practically reached. This can be seen by a simulation that instead of an LED uses a light source with an emission equal to the reflection of a Lamber-

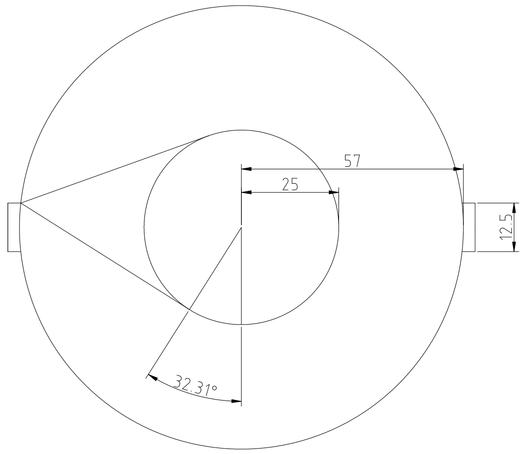

Figure 7.1: Sketch of the POCAM with a 12.5 mm waistband. Refraction between the glass and the interior is neglected. We see that the surface spanning from the bottom up to an angle of $\theta = 180° - 32.31°$ does not contribute to the light output of the upper hemisphere.

tian surface $I(\theta) \propto \cos\theta$. Figure 7.2 shows, that for the prototype sphere the anisotropy is only of the order of 10^{-3}.

On the other hand the anisotropy caused by unreflected photons can be calculated using simple statistics. With T the chance of being transmitted and R the chance of being reflected (we ignore any dependence on the angle for our approximation), the number of unreflected photons n_u is given by

$$n_u = n \cdot T \tag{7.1}$$

For the number of photons leaving the sphere with being at least once reflected, we have to sum over all possible numbers of reflections

$$n_r = n \cdot \sum_{i=1}^{\infty} R^i \cdot T = n \cdot \left(\sum_{i=0}^{\infty} R^i \cdot T - T \right) = nT \cdot \left(\frac{1}{1-R} - 1 \right) \tag{7.2}$$

$$\frac{n_u}{n_r} = \frac{1-R}{R} \tag{7.3}$$

Even for a high reflectivity of 99% this ratio lies above 0.01 and is at least one order of magnitude bigger than the anisotropy caused by reflected photons.

We can test this considerations on our measurements of the prototype. In Figure 7.3 details are explained, the results support the approximation that anisotropy is caused by unreflected photons.

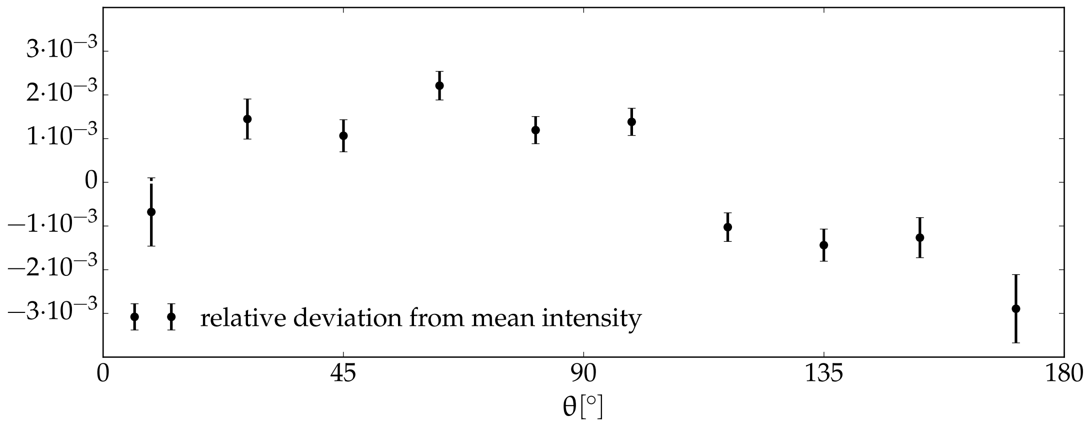

Figure 7.2: Simulation of the prototype integrating sphere ($R = 0.79$ and $T = 0.21$) for a source with Lambertian distribution sitting right at the lower border of the integrating sphere pointing upwards (towards $\theta = 0$). The simulation was done with $n = 7 \cdot 10^7$. Still the small bin number of 10 is necessary to compensate statistical noise. One sees that the anisotropy is only in the order of magnitude of 10^{-3}.

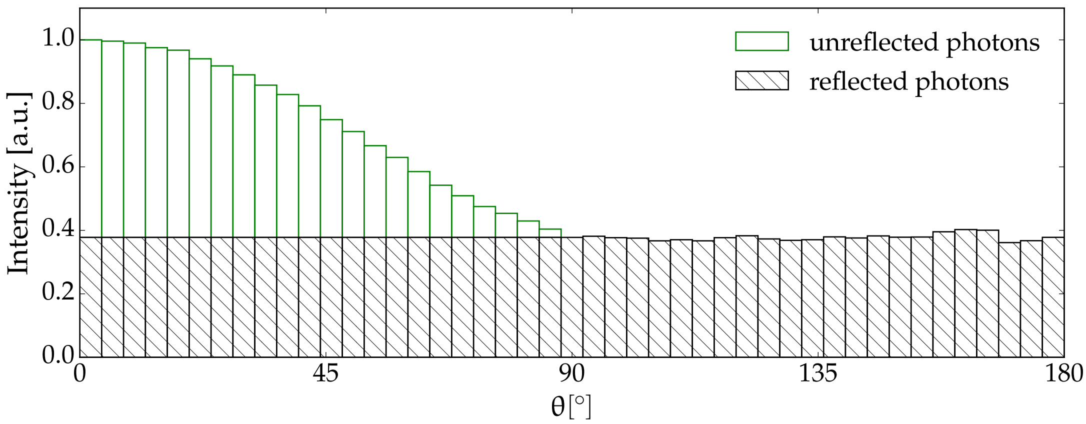

Figure 7.3: The same data as in Figure 5.4. Each bin below 90° is divided in a part caused by unreflected photons and an isotropic part caused by reflected photons. The dividing line was drawn at the mean of the bins with $\theta > 90°$. By weighting each bin with $\sin\theta$, the ratio of the sums equals $\frac{n_u}{n_r} = 0.32$ which corresponds to $R = 0.76$. Using the same method on the simulation from Figure 5.4 yields $R = 0.77$. Our measured value was $R = 0.79$, but since we assumed $A = 0$ (which is not given in reality nor in the simulation, where the LED and its cables absorb light) a slightly smaller value has to be expected.

To sum up, a good integrating sphere is defined by its high reflectivity, transmission and absorption play a subordinate role to isotropy. To compensate low reflectivity, the distribution of the unreflected photons should be as isotropic as possible, which means the LED should have a wide opening angle.

7.3 Light sources

For an integrating sphere with given reflectivity the anisotropy depends upon the light source, particularly on its angular intensity distribution, its size and its position. In Section 7.4 the size, being relevant as it can cast a large or small shadow, will not be considered for the LED only but also for general objects, since it is possible that screws are needed to mount the integrating sphere.

7.3.1 Opening angle and position

The theoretical considerations suggest that the anisotropy is caused by light leaving the sphere without being reflected. In an actual integrating sphere this can be seen as a bright spot on the side illuminated directly by the source. The goal should therefore be a large spot of low intensity. From this two simple rules follow: first, the light source should have an opening angle as wide as possible, second, the light source should be placed as far away as possible from the part of the sphere it illuminates. The simulations in Figure 7.4 show the expected behaviour. The flat head SMD LED is therefore the best choice, being placed with its bottom side as close to the wall as possible.

7.3.2 The SMD LED

We will now use the flat head SMD LED from the LED measurements in the preliminaries. Since the LED will be placed on some sort of board, possibly with other LEDs, everything above $\theta = 90°$ is cut of. The simulations in Figure 7.5 show better isotropy than the ideal light sources, as one would expect given the large opening angle. For the LED sitting only 1 mm above the bottom (corresponding $\Delta = 45$ mm distance to the top) a yet unseen sort of anisotropy appears. The drop of intensity is compensated by the short distance to points on the lower hemisphere, therefore it is actually brighter than the upper hemisphere. By carefully balancing between both hemispheres the deviation of the intensity can be lowered to 4% with the light source sitting 3 mm above the bottom ($\Delta = 43$ mm).

7.3.3 Lambertian light source

Section 7.2 has shown as a side result that a light source with the light distribution of a Lambertian surface sitting at the border of the sphere would be ideal. Although no LED has shown such behaviour, it could simply be realized by placing a thin sheet of PTFE over the LED. Such a light source would however not sit at the very border of the wall but slightly above it. Figure 7.6 shows the effect, the lower plot with a Lambertian light source sitting 1 mm above the bottom ($\Delta = 45$ mm from the top side) shows the best isotropy so far. The deviation between minimum and maximum might with 4% be as big

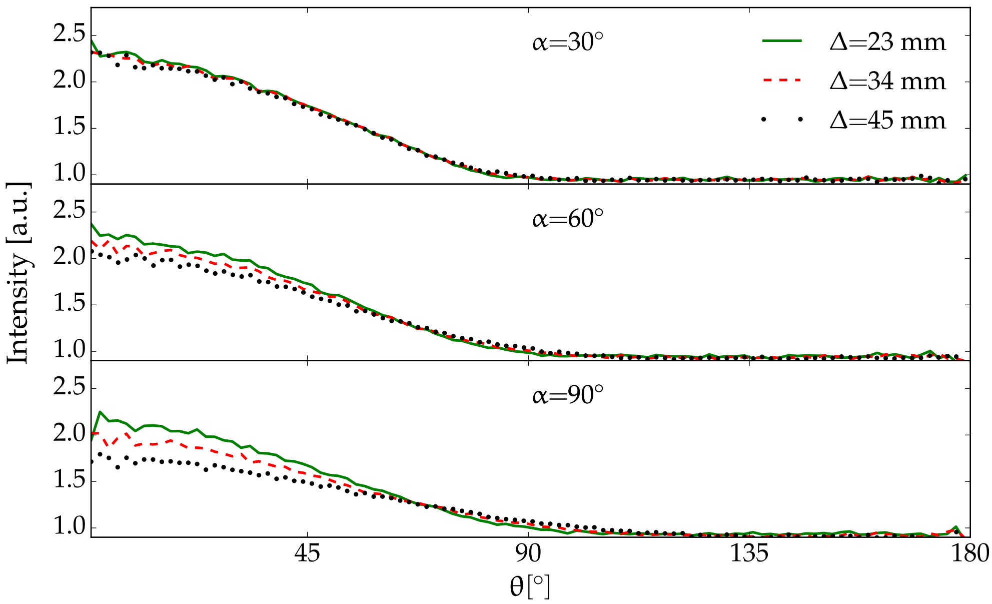

Figure 7.4: Simulation for different opening angles α and positions, where the light source is placed on the z-Axis pointing upwards. Δ is the distance between the light source and the upper wall of the sphere, $\Delta = 23$ mm means the source sits in the center, at $\Delta = 45$ mm the source sits 1 mm above the bottom of the sphere. A cosine-like angular distribution was simulated with $I(\theta) = 0.5 + 0.5\cos(180° \cdot \theta/\alpha)$, $\theta \leqslant \alpha$. The light source itself casts no shadow. For the integrating sphere we used the optical properties of the prototype ($R = 0.79$ and $T = 0.21$), each simulation was run with $n = 10^6$ photons. Each plot was normalized by setting the mean for $\theta > 120°$ to one as this part is isotropic.

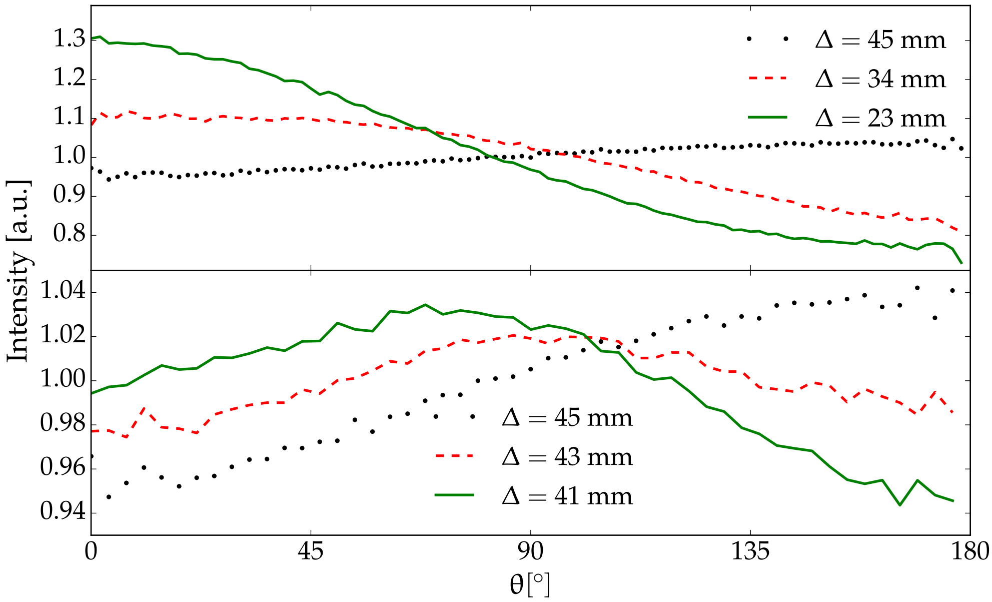

Figure 7.5: Simulations with $n = 10^7$ of the flat head LED. The best isotropy we can get comes with the distance $\Delta = 43$ mm to the top.

as the deviation for the flat head LED, the deviation in the upper hemisphere is however below 0.5%.

7.4 Internal objects

Every object inside the integrating sphere is naturally bound to cast a shadow. For the simulation it is not relevant what the exact purpose of this object is, we will just consider the general case. Any object at the wall of the integrating sphere will cause the part it covers to be dark on the outside. Any direction in which this dark spot can be seen will receive less light, therefore isotropy is not given anymore. To a simulation of an otherwise isotropic integrating sphere a small black object of 1 mm thickness is added, spanning from $\theta = 90°$ to $\theta = 90° - \alpha$ with $\alpha = 5°, 10°, 15°$. The simulation in Figure 7.7 shows that in order to limit the effect of the shadow to $\theta \leqslant 90°$ the object can not be much bigger than 5°, which for an inner sphere radius of 23 mm means the object should have no diameter above 4 mm.

7.5 Down facing light source

The profiles in Figure 7.4 show massive anisotropies that are however mostly confined to $\theta < 90°$. A simple solution would be to place the LED facing downwards and let the anisotropies be absorbed by the darkened lower hemisphere of the housing. In such a case a LED with a very small opening angle would be used to confine the anisotropies to the lower hemisphere. All light leaving the POCAM would therefore be at last once

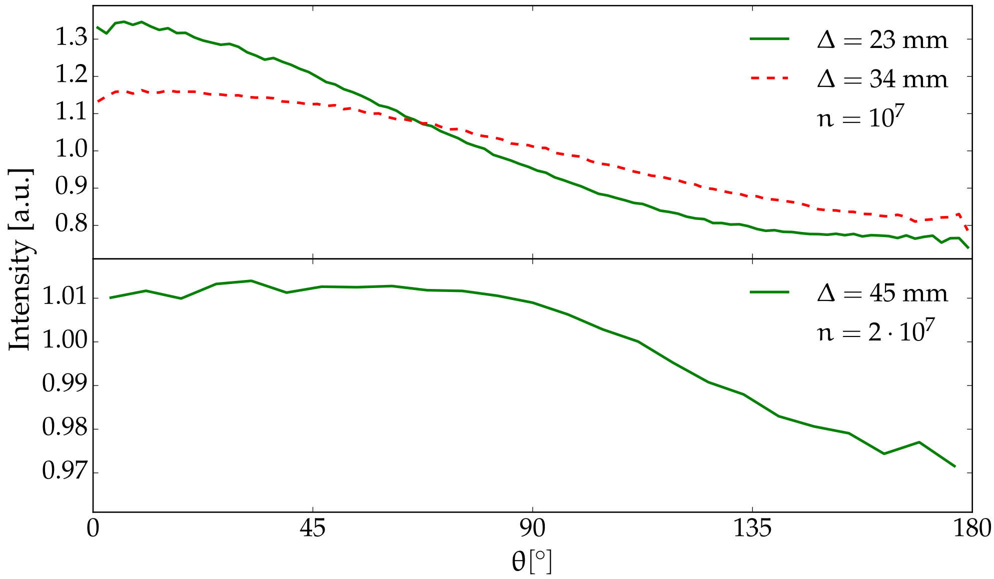

Figure 7.6: Simulations for a light source with $I(\theta) \propto \cos\theta$.

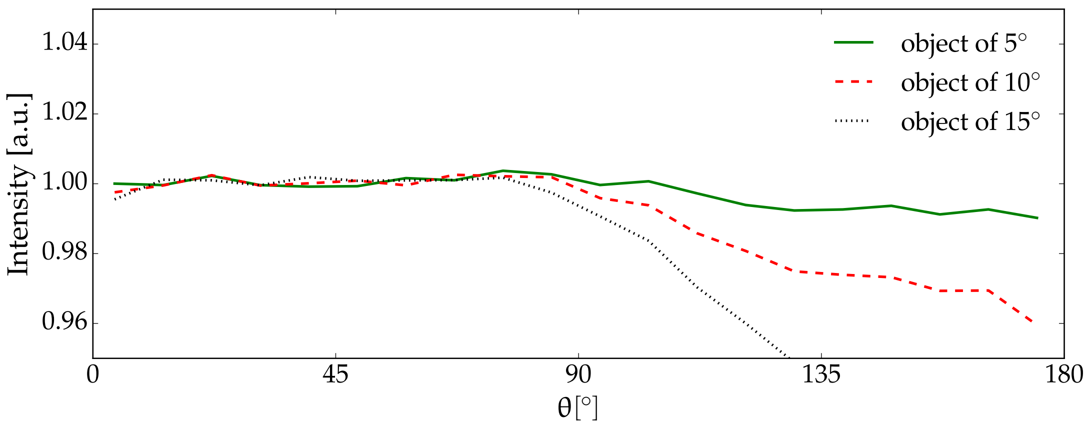

Figure 7.7: Simulations with $n = 10^7$ photons for a shadow casting object on the inner side of the integrating sphere wall.

reflected and the ideal isotropy of a Lambertian light source seen in Figure 7.2 would be reached. Practically the first reflection would take over the part that the light source had in previous simulations.

What seems to be an ideal solution is however very difficult to construct with respect to the cables of the LED. They can neither be placed outside of the integrating sphere, where they would cast a shadow, nor on the inner side of the wall for the same reason. If one were to place them in such a way that after entering the sphere from below they would rise with some distance to the walls, free standing so to say, they would cast a large shadow either to the direct light of the LED or to the light after its first reflection. The light source would be highly anisotropic in ϕ and an isotropic integrating sphere could no longer be reached.

7.6 Outer light source

Contrary to all previous considerations the light source has not to be placed inside the integrating sphere. Instead it could be placed close to a point at the outside and shine into the sphere through transmission. In this case the opening angle of the LED is not of much concern anymore. Sufficient isolating has to be ensured to prevent direct light from the light source from leaving the POCAM. One has to consider that due to the high reflectivity a large fraction of the light will be lost. This can be compensated by carefully thinning out the integrating sphere at this position by carefully drilling a hole in the size of the LED half way through the wall. This construction combines the benefits of a Lambertian light source with acceptance of practically any type of LED and is rather easy to build since nothing has to be placed inside the integrating sphere. That such a construction shows almost perfect isotropy was already seen in Fig. 7.2. It is therefore the construction we currently plan to use.

7.6.1 Measurements

For test measurements two PTFE spheres from a producer of PTFE ball bearings were obtained. The dimensions of the spheres are 25 mm radius with 1 mm thickness and 25 mm radius with 2 mm thickness. The latter version consists of two half spheres that can be joined with a screw coupling. This PTFE was optimized for mechanical purposes, we can therefore not simply compare it to a plain piece of PTFE of the same thickness as we did with the prototype sphere. Measurements without simulation have to be sufficient.

Additional measurements are done with our prototype integrating sphere (30 mm radius and 2 mm thickness). Additionally the 1 mm wall of a $r = 25$ mm sphere was carefully thinned to 0.4 mm at the light entry point. This will lead to a higher intensity as more light can enter the sphere.

To enable these measurements the measuring apparatus was slightly modified. A LED was placed inside a steel pipe that while being covered by black tape on the outside allowed reflections on the inside. The pipe was placed on a guide rail on which it could be adjusted in such a way that its opening touched the integrating sphere. The results can be seen in Figure 7.8.

The measurements show a significant problem, namely different behaviour for different rotations of the sphere to the light source. The reason for this are inhomogeneities in

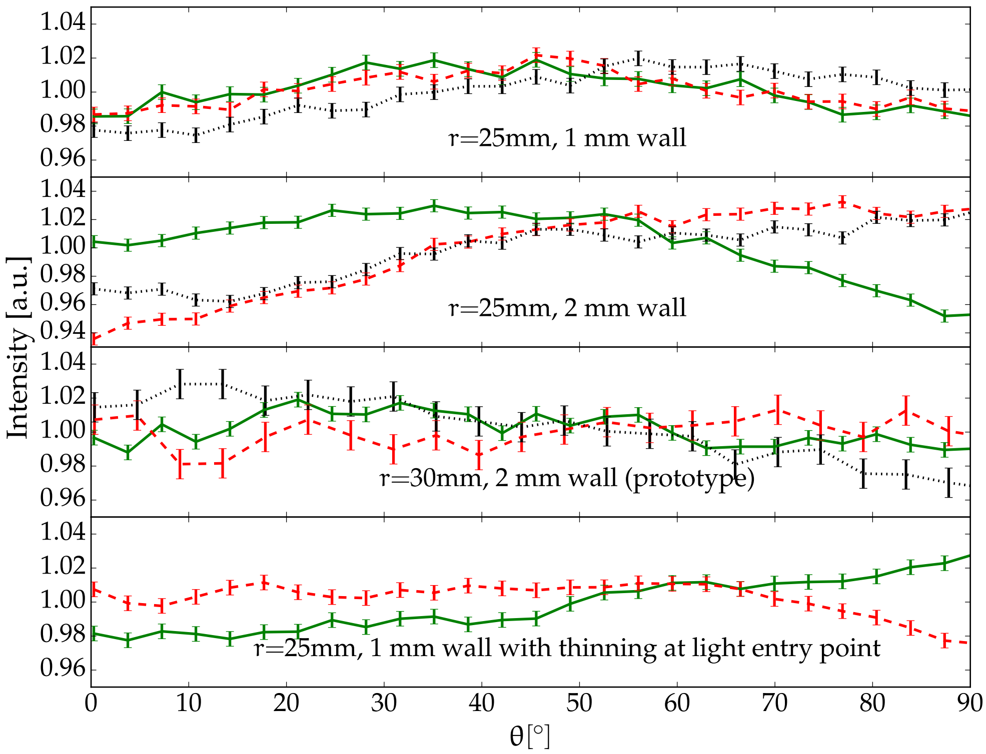

Figure 7.8: Measurements for the integrating spheres, the mean is normalized to 1. Each plot shows three measurements of the same integrating sphere but for different rotations of the sphere while the light source always points towards $\theta = 0°$. An exception was made for the last plot since rotating the sphere makes no sense if it is only thinned out at one point. Here two different spheres were measured. $\theta > 90°$ was cut off since the shadow of the measuring apparatus affects this region.

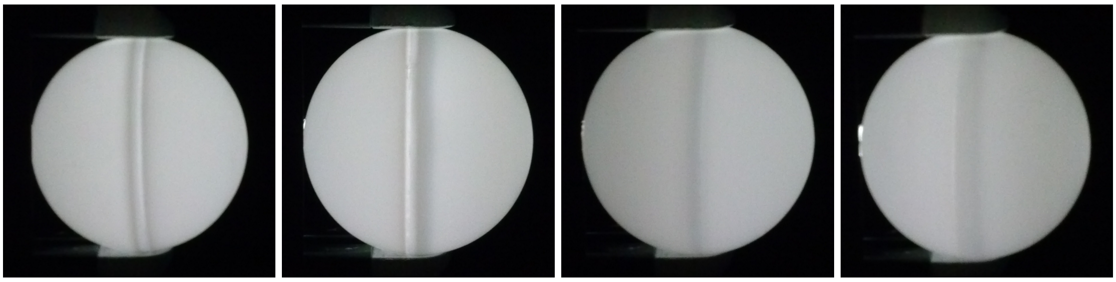

Figure 7.9: Photos of the illuminated integrating spheres, the light enters the sphere from the left in all photos. From left to right: $r = 25$ mm, 1 mm wall; same sphere rotated by 180°; $r = 25$ mm, 2 mm wall; same sphere rotated by 180°. For the 2 mm wall we see the screw coupling, for the 1 mm wall we see where the manufacturer welded two half spheres together. Also the different brightness of the half spheres is visible.

the PTFE that can be seen with the unaided eye if a strong light source illuminates the sphere (Fig. 7.9). If deviations of 5% are acceptable, the thinned 1 mm PTFE sphere can be used. Otherwise further testing of different spheres from different suppliers is needed.

Of additional interest is the absolute brightness of the sphere. Figure 7.10 shows the intensities for the discussed spheres. For comparison the prototype sphere with the LED inside from an earlier chapter was also plotted. We see as expected that the highest brightness is reached for the thinned sphere. Above all the measurements show that an outer light source does not need to result in a darker integrating sphere.

7.7 Mounting the integrating sphere

One of the outstanding properties of PTFE is that few substances are able to stick to it. Tests with glues have shown that gluing is not the way to mount the integrating sphere. A simple solution would be to screw it using a single small screw. Still it would be better to have a way of mounting the sphere without having to place objects inside of it, especially since Section 7.6 has shown that not even the light source has to be in the interior.

To hold the sphere by purely mechanical means a little notch is carved around the sphere at $\theta = 155°$ in accordance to the limit determined in Section 7.1. Glue can flow into this notch and will after drying hold the integrating sphere just by its own mechanical stability (Fig. 7.11). This way the integrating sphere can be glued to a pipe that sits on the main electronics board. A test setup was able to withstand at least a short time force of 10 N and a long time force of 5 N even after being exposed to a temperature difference of at least 20° C (from room temperature to below 0° C and back). For the final setup it has to be ensured that glue and pipe have the same thermal expansion coefficient as PTFE.

If the setup with no objects inside the integrating sphere is used, the idea of simply using an unpenetrated sphere could come up. One has to consider though that at least a small hole in the sphere is needed for pressure equalization. Ideally the hole in placed inside the area encompassed by the mounting tube. This of course requires sufficient light isolation from the LEDs and an additional hole in the main board.

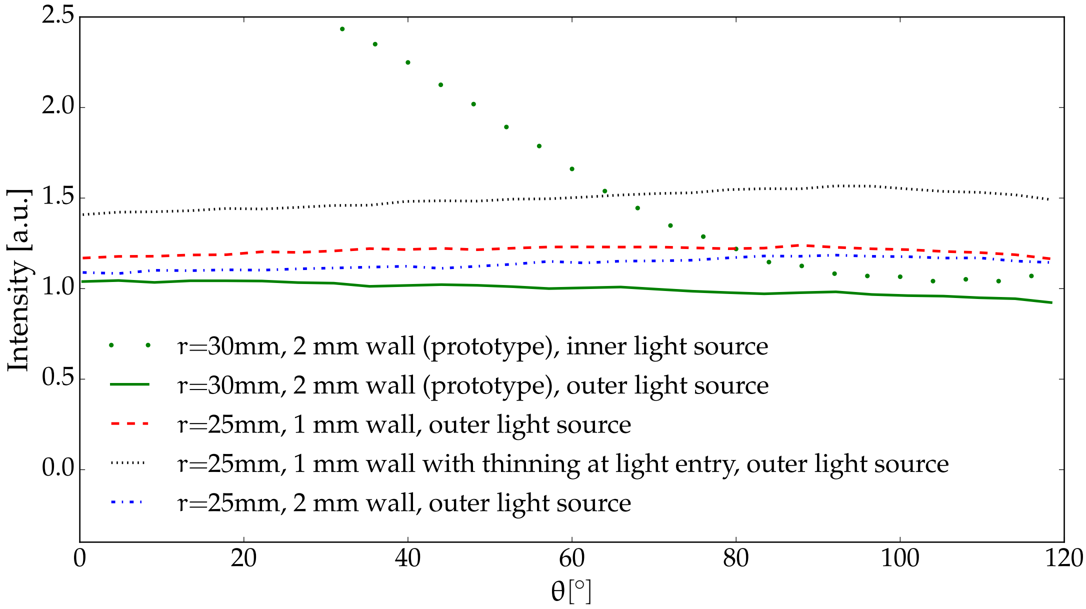

Figure 7.10: Measurements for the integrating spheres showing the different intensities, all were multiplied with the same factor to set the mean of the lowest to one.

Figure 7.11: Sketch and image of the integrating sphere mounting. The sketch is not true to scale.

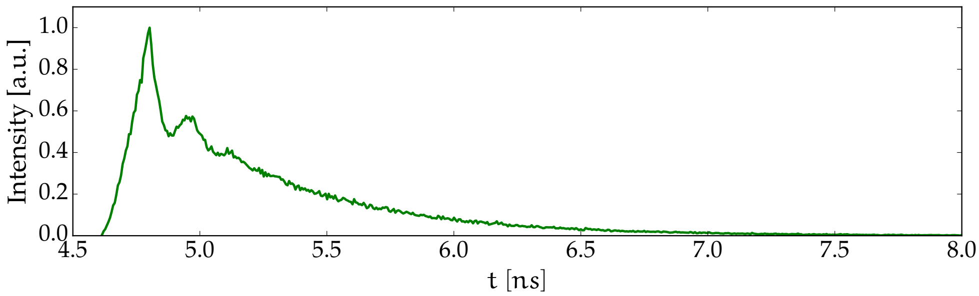

Figure 7.12: The final time profile P_δ when starting with a δ-distribution. At the beginning one can distinguish peaks for unreflected photons and photons that were one, two or three times reflected. Please note that the offset of circa 4.6 ns is based on the 1 m of ice that surrounds the POCAM in all simulations. The simulation was done with $n = 10^7$ photons.

7.8 Time profiles

Whereas previous chapters dealt only with the angular distribution, the time profile of the light is also of enormous importance. Of the many parts of the POCAM the integrating sphere, the LED and the Kapustinsky circuit are responsible for the time profile. We will differ between the initial time profile p of the LED and the final time profile of the integrating sphere P. Since the testing of different LEDs and circuit configurations is still in progress, we will simulate the LED time profile as a delta peak. The advantage of this is that the final time profile of the integrating sphere for any LED can then be simply obtained by folding the LEDs time profile with the final profile of the delta peak, which can be explained as follows: Since photons do not interact with each other the final profile of a sum of initial profiles is the sum of their final profiles.

$$p_i(t) \to P_i(t) \tag{7.4}$$

$$\sum_i p_i(t - t_i) \to \sum_i P_i(t - t_i) \tag{7.5}$$

Since an integral behaves like a sum we get for an arbitrary initial profile p_{LED}

$$p_{LED}(t) = \int d\tau\, \delta(t - \tau) p_{LED}(\tau) \to \int d\tau\, P_\delta(t - \tau) p_{LED}(\tau) = (p_{LED} * P_\delta)(t) \tag{7.6}$$

We can now simulate the time profile for our integrating sphere setup with PTFE of $R = 0.79$ and $T = 0.21$. Of course the simulation needs to be rerun if PTFE with different T and R will be used. The housing is only traversed once by the light, its only effect is a delay of the signal. The following plots show the time profiles P_δ (Fig. 7.12), p_{LED} (Fig. 7.13) and $P_{LED} = p_{LED} * P_\delta$ (Fig. 7.14), each separately normalized so that the maximum equals 1.

The simulation shows that the integrating sphere does not overly stretch the signal since its width (FWHM $\approx$ 0.3 ns) is much smaller than the width of the initial pulse (FWHM $\approx$ 5 ns).

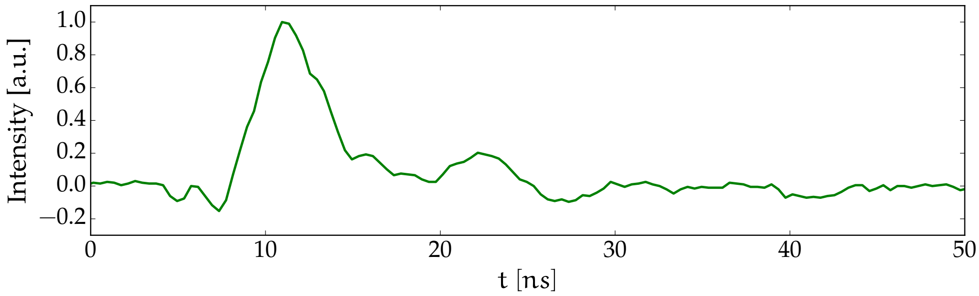

Figure 7.13: The initial time profile of a LED p_{LED} in a Kapustinsky circuit. Measured by Antonio Becerra Esteban of the TUM ECP group.

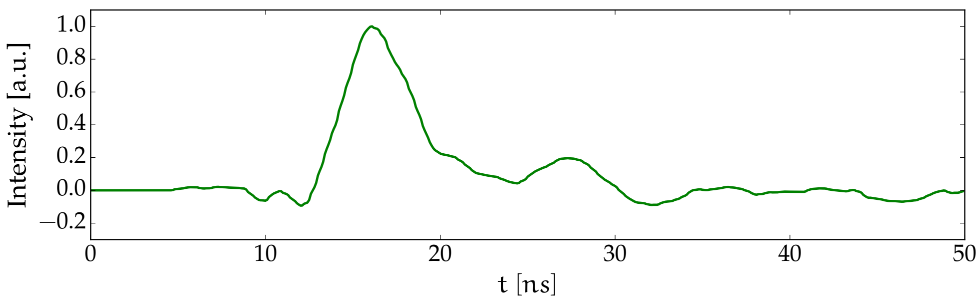

Figure 7.14: The final time profile of the LED P_{LED}, obtained by folding P_δ and p_{LED}.

Chapter 8

Light propagation through ice

In order to use the POCAM to calibrate PINGU, the propagation through ice needs to be simulated. For this CLAIM can be used, a software produced by the IceCube Collaboration for photon tracking using elaborate models of the South Pole ice, including depth dependent optical properties and special treatment of the refrozen drill holes.

8.1 Pixelization

Unlike Geant4 the CLSIM software can not simulate large numbers of single photons. Groups of photons are simulated instead of single photons which then propagate with certain directional deviations. The number of groups is the factor limited by computing power.

When applying the output of a Geant4 simulation with photon numbers of $10^7 - 10^8$ a reasonable way for grouping is necessary. The most convenient way to do so is again the use of the HEALPix pixelization. The most precise result would be obtained using the largest number of pixels possible, the used computer can simulate up to $2 \cdot 10^6$ groups, the closest smaller HEALPix order would be 8 with $12 \cdot 4^8 \approx 8 \cdot 10^5$ bins.

8.1.1 Artifacts

The main disadvantage of any pixelization are Pixelization artifacts. If the broad spectrum of possible photon directions is broken down to few discrete values, an isotropic light source can no longer be simulated as isotropic. If we pixelate the POCAM output with order 8 we get an angular resolution of $0.2°$. The scattering coefficient of the deep Antarctic ice for depths from 1400 to 2000 meter can be as small as $b = 0.2\ \mathrm{m}^{-1}$ [12]. The length light travels before it is scattered can therefore be roughly estimated with $L = b^{-1} = 50$ m. The $0.2°$ correspond in this distance to 20 cm, which is in the order of magnitude of the DOM size (33 cm diameter) and therefore a not negligible deviation. Hence for precise simulations more elaborate algorithms have to be found especially since many DOMs of the PINGU upgrade lie in this distance to the planned POCAM position.

8.2 Provisional simulation

To get a simple overview over the light propagation through ice the following plots show two simulations, one with the POCAM pointing upwards and one with it pointing downwards. Instead of pixelating the output of a Geant4 simulation an isotropic half sphere was used as light source.

In the simulation the POCAMs are placed in the middle of PINGU in the place of DOM 48 on string 88. Due to the hexagonal grid of PINGU many strings have the same distance to the POCAM string. For the plots the mean of all such strings was taken. A pulse from the Kapustinski circuit produces $10^7 - 10^8$ photons, the simulations ran with 10^7 photons. To reduce statistical noise 200 simulations were done each and the mean was taken.

The results in Figure 8.1 show that a POCAM pointing up has a higher measured photon number since the DOM photomultiplier tubes are pointing downwards. Only very few photons reach the upper and lower and of PINGU, a large number of flashes will therefore be necessary to properly calibrate it. The most distant DOMs show an average photon number of 0.01. If the calibration error should be smaller than 5% then at least $(1/0.05)^2$ photons need to be detected. The number of necessary flashes lies therefore in the order of 10^5.

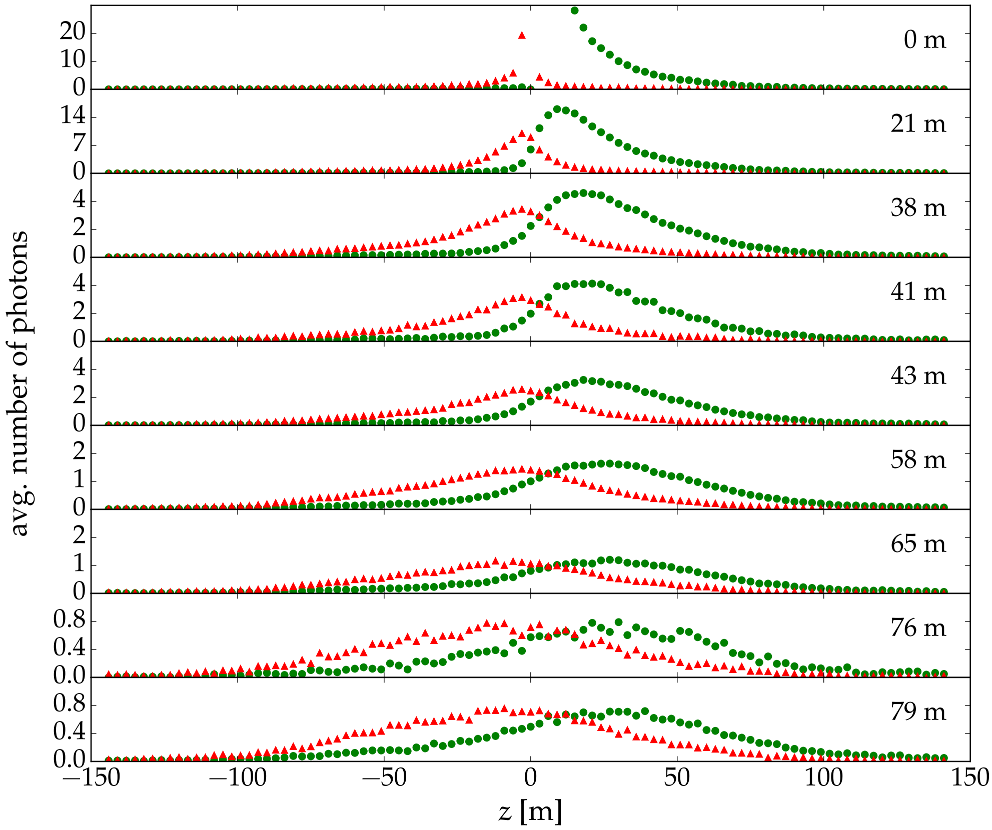

Figure 8.1: CLSIM simulation for a POCAM pointing down (red) and a POCAM pointing up (green). The average number of detected photons for each DOM was plotted. The number in the top right corner gives the distance of the string to the POCAM string, z is the difference between the depth of the DOM and the depth of the POCAM.

Chapter 9

Conclusion and outlook

The previous chapters have shown that the POCAM can be realized as almost isotropic in one hemisphere, with deviations of 5% and a shadow from the main cable whereas two POCAMs are necessary to illuminate 4π. Enough space is available for multiple LEDs and their respective electronics allowing different wavelengths and pulse lengths and the light pulse of the LED is not significantly elongated by the integrating sphere. The opening angle of the LED plays no role if the setup with the light source outside of the integrating sphere is used.

Chapter 6 has shown that the integrating sphere should be placed in the middle of the housing. With the measurements from Chapter 7 the use of optical gel seems unlikely as its contributions to the isotropy are much smaller than the deviations caused by PTFE inhomogeneities.

9.1 Further steps of construction

While the electronics are still under active consideration the next step could be the realization and testing of different hanging assemblies. If possible, additional integrating spheres should be tested and a prototype main board can be produced that without having to contain the Kapustinski circuit or a microcontroller might have some components allowing to test the data plug and cable. The most important step however is the testing of the housing under high pressure.

9.2 Lake Baikal

Presumably a test before the deployment in the ice can be done at lake Baikal in Russia in collaboration with the Baikal Deep Underwater Neutrino Telescope. It will allow to test the POCAM under high pressure and recollect it afterwards for detailed analysis.

Acknowledgements

I have to express my sincerest gratitude to the many people who helped me during my work on this thesis. To Prof. Elisa Resconi who allowed me to work in her group and gave helpful advice and support it goes as well as to Kilian Holzapfel and his valuable guidance, to Felix Henningsen, without whom the POCAM would still be only a simulation and to Kai Krings and his programming expertise. And so it includes Joost Veenkamp's help and instructions, Dr. Roman Gernhäuser with his knowledge in bringing mere concepts into reality and Ralf Lang and Michael Klöckner who expertly created the many parts needed for testing and measurements. I would also like to thank Stefan Coenders and Andrea Turcati for providing the most valuable feedback to this thesis.

Bibliography

[1] C. L. Cowan et al., *Detection of the Free Neutrino: a Confirmation*. Science 20 Jul 1956 Vol. 124, Issue 3212, pp. 103-104.

[2] M. G. Aartsen et al. (IceCube Collaboration), *Energy Reconstruction Methods in the IceCube Neutrino Telescope*. JINST 9 (2014), P03009.

[3] B. T. Cleveland et al. (SNO Collaboration), *Measurement of the solar electron neutrino flux with the Homestake chlorine detector*. Astrophys.J. 496 (1998) 505-526.

[4] Q. R. Ahmad et al. (SNO Collaboration), *Measurement of the rate of* $\nu_e + d \rightarrow p + p + e^-$ *interactions produced by* ^8B *solar neutrinos at the Sudbury Neutrino Observatory*. Phys.Rev.Lett.87:071301,2001.

[5] T. K. Gaisser, R. Engel, E. Resconi, *Cosmic rays and particle physics*. Cambridge University Press, 2016.

[6] M. G. Aartsen et al. (IceCube Collaboration), *Evidence for High-Energy Extraterrestrial Neutrinos at the IceCube Detector*. Science 342, 1242856 (2013).

[7] K. A. Olive et al. (Particle Data Group), *Review of Particle Physics*. Chinese Physics C Vol. 38, No. 9 (2014) 090001.

[8] R. Abbasi et al., *Measurement of the anisotropy of cosmic-ray arrival directions with IceCube*. The Astrophysical Journal Letters, Volume 718, Number 2.

[9] R. Abbasi et al. (IceCube Collaboration), *IceTop: The surface component of IceCube*. NIM A700:188,2013.

[10] L. Fabietti, D. Straub, *Kern-, Teilchen- und Astrophysik 2*. Lecture series held at TUM in the summer semester of 2016.

[11] R. Abbasi et al. (IceCube Collaboration), *Calibration and Characterization of the IceCube Photomultiplier Tube*. Nucl.Instrum.Meth.A618:139-152,2010.

[12] M. Ackermann et al., *Optical properties of deep glacial ice at the South Pole*. Journal of Geophysical Research, vol. 111, D13203, doi:10.1029/2005JD006687, 2006.

[13] M. G. Aartsen et al. (IceCube Collaboration), *Measurement of South Pole ice transparency with the IceCube LED calibration system*. NIM A711:73,2013.

[14] M. G. Aartsen et al. (IceCube Collaboration), *Measurement of South Pole ice transparency with the IceCube LED calibration system*. NIM A711:73,2013.

[15] R. Abbasi et al. (IceCube Collaboration), *The IceCube Data Acquisition System: Signal Capture, Digitization, and Timestamping*. Nucl.Instrum.Meth.A601:294-316,2009.

[16] M. G. Aartsen et al. (IceCube-Gen2 Collaboration), *IceCube-Gen2: A Vision for the Future of Neutrino Astronomy in Antarctica*. arXiv:1412.5106v2 [astro-ph.HE] 18 Dec 2014.

[17] M. G. Aartsen et al. (IceCube-PINGU Collaboration), *Letter of Intent: The Precision IceCube Next Generation Upgrade (PINGU)*. arXiv:1401.2046 (2014).

[18] Hamamatsu Photonics, *Hamamatsu Data Sheet, Nov. 12. 2003, Photomultiplier tube R7081-02 for ICECUBE Experiments*.

[19] P. B. Price and K. Woschnagg, *Role of Group and Phase Velocity in High-Energy Neutrino Observatories*. Astropart.Phys.15:97-100, 2001.

[20] A. Karle, K. Woschnagg, *Hole Ice Studies with YAG data/MC*. retrieved 21.07.16 from http://icecube.berkeley.edu/kurt/interstring/hole-ice/yak.html.

[21] Schott AG, *Datenblatt Schott N-BK 7 517642.251, 01.02.2014*.

[22] S. Agostinelli et al., *GEANT4: A Simulation toolkit*. Nucl.Instrum.Meth. A506 (2003) 250-303.

[23] K. M. Gorski, *The HEALPix Primer*. arXiv:astro-ph/9905275 (1999).

[24] B. K. Lubsandorzhiev, Y. E. Vyatchin, *Studies of "Kapustinsky's" light pulser timing characteristics*. JINST 1 (2006) T06001.

[25] J. S. Kapustinsky et al., *A fast timing light pulser for scintillation detectors*, 1985. Nucl. Instrum. Meth., vol. A241, p. 612-613.

[26] LITE-ON Technology Corporation, *SMD LED Product Data Sheet*, 11 2011. Rev. L.